DCAF1 regulates Treg senescence via the ROS axis during immunological aging

Zengli Guo,[1,2] Gang Wang,[1,2,3] Bing Wu,[1,2] Wei-Chun Chou,[1,4] Liang Cheng,[1,2] Chenlin Zhou,[1] Jitong Lou,[5] Di Wu,[5,6] Lishan Su,[1,2] Junnian Zheng,[3] Jenny P.-Y. Ting,[1,2,4] and Yisong Y. Wan[1,2]

[1]Lineberger Comprehensive Cancer Center and [2]Department of Microbiology and Immunology, School of Medicine, University of North Carolina at Chapel Hill, Chapel Hill, North Carolina, USA. [3]Jiangsu Center for the Collaboration and Innovation of Cancer Biotherapy, Cancer Institute, Xuzhou Medical University, Xuzhou, China. [4]Department of Genetics, [5]Department of Biostatistics, Gillings School of Global Public Health, and [6]Department of Periodontology, School of Dentistry, University of North Carolina at Chapel Hill, Chapel Hill, North Carolina, USA.

As a hallmark of immunological aging, low-grade, chronic inflammation with accumulation of effector memory T cells contributes to increased susceptibility to many aging-related diseases. While the proinflammatory state of aged T cells indicates a dysregulation of immune homeostasis, whether and how aging drives regulatory T cell (Treg) aging and alters Treg function are not fully understood owing to a lack of specific aging markers. Here, by a combination of cellular, molecular, and bioinformatic approaches, we discovered that Tregs senesce more severely than conventional T (Tconv) cells during aging. We found that Tregs from aged mice were less efficient than young Tregs in suppressing Tconv cell function in an inflammatory bowel disease model and in preventing Tconv cell aging in an irradiation-induced aging model. Furthermore, we revealed that DDB1- and CUL4-associated factor 1 (DCAF1) was downregulated in aged Tregs and was critical to restrain Treg aging via reactive oxygen species (ROS) regulated by glutathione-*S*-transferase P (GSTP1). Importantly, interfering with GSTP1 and ROS pathways reinvigorated the proliferation and function of aged Tregs. Therefore, our studies uncover an important role of the DCAF1/GSTP1/ROS axis in Treg senescence, which leads to uncontrolled inflammation and immunological aging.

Introduction

Immunological aging is associated with declined immunity (immunosenescence) and chronic nonspecific inflammation (inflammaging) (1), contributing to age-associated morbidities and mortalities, including infection, cancer, and autoimmunity, which are detrimental to the health of aging populations globally (2–4). Chronic inflammation not only accelerates immunological aging (5), but also contributes to a variety of aging-related diseases (6) such as Alzheimer's disease (7, 8). Thus, targeting chronic inflammation, by using genetic and pharmacological approaches, has been an important strategy to extend healthspan and lifespan across species (9). As one of the most basic changes in immunological aging, the accumulation of excessive effector memory T cells exists in both aged humans and aged pathogen-free mice (10, 11), with poorly defined mechanisms.

The proper function of the immune system can only be achieved by well-balanced immune activation and immune suppression, as the disruption of immune homeostasis often leads to health issues and diseases (12). Because conventional T cells (Tconv cells) activate immune responses and regulatory T cells (Tregs) suppress them (13), effector memory T cell accumulation during aging could be due to either enhanced Tconv cell function or reduced Treg function. The former possibility seems less likely, because it is generally agreed that the function of Tconv cells is not enhanced, and may worsen, with aging (14), which contributes to compromised vaccination and a decline in immunity against tumors and infections in the aged population (15). However, the latter possibility, that defects in Treg function lead to aging-related inflammation, remains unclearly defined (16).

Previous studies found that the function of aged Tregs appeared to be unaltered or even increased (17–19). Yet later studies suggested that aged Tregs may be less effective in suppressing the function of Tconv cells in vitro (20) and in expanding in response to muscle injury in vivo (21), implying that aging may negatively influence the intrinsic function of Tregs. Therefore, whether and how the intrinsic function of Tregs may alter during aging to influence immunological aging remains a question to be clearly elucidated (22).

Here we investigated the intrinsic function of Tregs during aging and discovered that Tregs senesce more severely than Tconv cells with age, with a preferential upregulation of the senescence-related molecular program. Compared with non-aged Tregs, aged Tregs were less efficient in proliferating and in suppressing Tconv cell function both in vitro and in an inflammatory bowel disease model. Consequently, aged Tregs failed to prevent Tconv cell aging in an irradiation-induced immunological aging model when compared with young Tregs. In addition, we discovered that DDB1- and CUL4-associated factor 1 (DCAF1) was critical in restraining Treg aging via its interaction with glutathione-*S*-transferase P (GSTP1), an enzyme that plays an important role in buffering reactive oxygen species (ROS) by catalyzing intracellular detoxification reactions. Moreover, we revealed that

Conflict of interest: The authors have declared that no conflict of interest exists.
Submitted: January 15, 2020; **Accepted:** July 29, 2020; **Published:** October 5, 2020.
Reference information: *J Clin Invest*. 2020;130(11):5893–5908.
https://doi.org/10.1172/JCI136466.

the ROS-related program was preferentially upregulated in aged Tregs, and, importantly, interfering with GSTP1 and ROS pathways reinvigorated the proliferation and function of aged Tregs.

Results

Preferential Treg aging in comparison with Tconv cells in young and aged mice. We comprehensively analyzed T cell function in aged (>18 months old) mice. Tconv cells in aged mice adopted effector memory phenotypes (Supplemental Figure 1, A–D; supplemental material available online with this article; https://doi.org/10.1172/JCI136466DS1), a hallmark of immunological aging, as expected (10). While aged Tconv cells were not intrinsically more sensitive to T cell receptor–activated proliferation compared with their young counterparts, aged Tregs proliferated much less than young Tregs (Figure 1A), when they were cocultured under the same conditions to exclude cell extrinsic influences. The proliferative defect of aged Tregs consistently existed in assays by either CFSE dilution or BrdU incorporation (Figure 1A and Supplemental Figure 1E), regardless of the presence or absence of Tconv cells (Supplemental Figure 1, F and G) or the strength of T cell receptor stimulation (Supplemental Figure 1H). This finding is quite unexpected as the proportion of Tregs was found to be increased in aged mice (refs. 18, 20, 23, and Supplemental Figure 1I), which could be due to Treg expansion driven by chronic inflammation (24). Consistent with the reduced proliferative capacity, aged Tregs displayed high senescence-associated β-galactosidase (SA-β-gal) activity (Figure 1B), a hallmark of cellular senescence (25). Unbiased genome-wide RNA-Seq analysis identified genes that were differentially regulated in aged Tregs compared with their young counterparts to reveal an enrichment of the aging-related program (ref. 26 and Figure 1C) and preferential upregulation of senescence signature genes including *p16*^{Ink4a}, *p19*^{Arf}, and *p21*^{Cip1} (Figure 1, D and E, and Supplemental Table 1) in aged Tregs. Interestingly, genome-wide RNA-Seq analysis also revealed that the aging-related program was preferentially upregulated in Tregs compared with Tconv cells regardless of age (Figure 1, E and F), in agreement with the previous study on human T cells showing that Tregs have shorter telomeres than Tconv cells in both young and old donors (19). Therefore, compared with Tconv cells, Tregs manifest a more severe aging phenotype with deteriorated proliferative capacity during aging.

Deterioration of Treg function in aged mice. Whether and how aging influences Treg function remain unclearly defined (18, 20, 27–29). Our findings that aged Tregs showed defective proliferation and exacerbated senescence prompted us to comprehensively evaluate the intrinsic function of aged Tregs in vitro and in vivo. The suppression assay performed in vitro showed that, while young Tregs efficiently suppressed Tconv cell proliferation, aged Tregs were inferior in doing so (Figure 2A). In addition, fewer Foxp3$^+$ aged Tregs than young Tregs were recovered in the culture (Figure 2B), consistent with the impaired proliferative capacity of the aged Tregs (Figure 1A and Supplemental Figure 1, E, G, and H). Next, we analyzed Treg function in vivo using a naive CD4$^+$ T cell–induced colitis model (ref. 30 and Figure 2C). Similarly to what was observed in vitro, aged Tregs failed to protect mice from naive T cell–elicited colitis compared with young Tregs (Figure 2D). Our unbiased genome-wide RNA-Seq analysis revealed that aged Tregs expressed normal levels of Treg signature genes (*Foxp3*, *Tnfrsf18* encoding GITR, *Ikzf2*, *Il2ra*, *Capg*) and increased expression of key inflammatory cytokines (*Il1a*, *Il1b*, *Il4*, *Il6*, *Il17a*, *Il17f*), while the expression of B7 receptor family members, chemokine receptors, and Bcl2 family members was not uniformly changed in aged Tregs (Supplemental Figure 2A). This result indicates that aging reprograms Treg function via multiple mechanisms to contribute to a reduction of Treg expansion in vitro (Figure 2B) and in vivo (Figure 2E and Supplemental Figure 2B) and to a decrease in survival (Supplemental Figure 2C).

Based on the results above, we hypothesized that Tregs can restrain immunological aging and such an ability of Tregs declines when they age. To test this, we adopted an irradiation-induced immunological aging model (31) to compare the ability of young and aged Tregs to inhibit Tconv cell aging (Figure 2F). Low-dose irradiation effectively reduced the naive T cell population (Figure 2G, left) and induced Tconv cell aging marked by *p16*^{Ink4a} upregulation (Figure 2G, right), resembling immunological aging. While the transferred young Tregs could efficiently inhibit the Tconv cell aging phenotype, aged Tregs were inferior in doing so (Figure 2G) and were poorly maintained in the periphery (Figure 2H). Compared with Tconv cells, Tregs are more prone to aging and function deterioration.

DCAF1 deletion leads to T cell aging in young mice. We next explored the potential factors that control Treg aging and found that protein expression of DCAF1, a factor downregulated in aging tissues (ref. 32 and Supplemental Figure 3A), was also reduced in aged Tregs (Figure 3A). DCAF1 could be of interest because it is targeted by HIV (33) and controls p53 function (34), both of which contribute to immunological aging (35–37). We deleted DCAF1 specifically in T cells in *Cd4-Cre Dcaf1*$^{fl/fl}$ mice (34). DCAF1 deletion in T cells led to elevated SA-β-gal activity in both Tregs and Tconv cells even in young *Cd4-Cre Dcaf1*$^{fl/fl}$ mice, with the highest SA-β-gal activity observed in Tregs (Figure 3B). Heatmap and Pearson's correlation analysis of RNA-Seq data sets revealed that Dcaf1-deficient Tregs in young mice adopted an expression profile similar to that of WT aged Tregs when compared with young Tregs (Figure 3C). In addition, while DCAF1 deletion led to a global upregulation of the aging-related program and senescence signature genes in both Tconv cells and Tregs (Figure 3D), such an aging phenotype appeared to be more pronounced in Tregs (Figure 3E). Therefore, DCAF1 is essential to restrict the aging program of T cells and particularly Tregs.

DCAF1 is required to restrain Treg aging. Because T cell homeostasis of *Cd4-Cre Dcaf1*$^{fl/fl}$ mice was perturbed (34), the Treg phenotype observed in these mice could be confounded by the defects in Dcaf1-deficient Tconv cells. To investigate DCAF1 function in Tregs specifically, we bred *Dcaf1*$^{fl/fl}$ mice with *Foxp3-GFP-Cre* (FGC) mice to delete DCAF1 exclusively in Tregs in *FGC Dcaf1*$^{fl/fl}$ mice (Supplemental Figure 3B). Even though the Treg population appeared not to be affected (Supplemental Figure 3C), the function of Tregs was impaired, as Tconv cells displayed activated phenotypes including increased effector memory T cell populations and aberrant cytokine production in young *FGC Dcaf1*$^{fl/fl}$ mice (Figure 4, A–D), a phenotype similar to those in aged mice and *Cd4-Cre Dcaf1*$^{fl/fl}$ mice. Additionally, *FGC Dcaf1*$^{fl/fl}$ mice ultimately developed splenomegaly and autoimmunity at the age of 7 months (Fig-

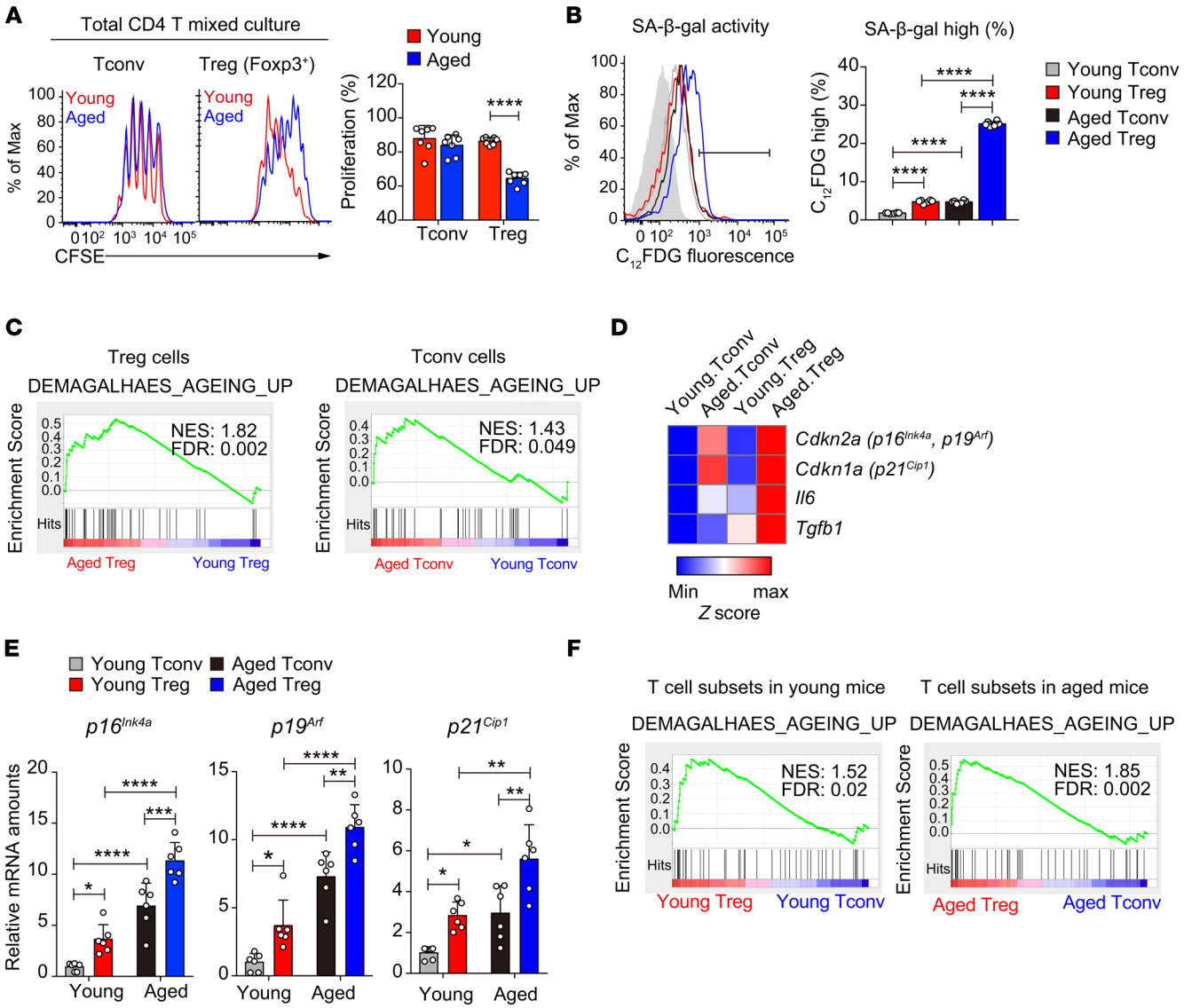

Figure 1. Preferential Treg aging in young and aged mice. (**A**) Proliferation of CD4$^+$Foxp3$^+$ (Treg) and CD4$^+$Foxp3$^-$ (Tconv) cells from young and aged (more than 18-month-old) mice 3 days after activation when cultured in the same well, analyzed by CFSE dilution and flow cytometry (n = 7 mice of 3 experiments; representative results are shown; means ± SD, $^{****}P < 0.0001$, by 1-way ANOVA followed by Tukey's multiple-comparisons test). (**B**) SA-β-gal activity of CD4$^+$CD25$^+$ Tregs and CD4$^+$CD25$^-$ Tconv cells in splenocytes from young and aged mice, assessed by flow cytometry with the fluorescent β-gal substrate C_{12}FDG (gray area, no C_{12}FDG; n = 6 mice of 3 experiments; representative flow cytometry results are shown; means ± SD, $^{****}P < 0.0001$, by 1-way ANOVA followed by Tukey's multiple-comparisons test). (**C**) Elevated aging program in aged Tregs (left panel) and aged Tconv cells (right panel) revealed by GSEA of RNA-Seq data sets. (**D** and **E**) Preferential upregulation of senescence signature genes in aged Tregs, revealed by heatmap analysis of RNA-Seq data sets (**D**) and by quantitative reverse transcriptase PCR (qRT-PCR) analysis of indicated genes (n = 6 mice of 3 experiments; means ± SD, $^*P < 0.05$, $^{**}P < 0.01$, $^{***}P < 0.001$, $^{****}P < 0.0001$, by 1-way ANOVA followed by Tukey's multiple-comparisons test) (**E**). (**F**) Preferential upregulation of the aging program in Tregs in both young (left) and aged (right) mice, revealed by GSEA of RNA-Seq data sets.

ure 4, E and F). Compared with WT Tregs, Dcaf1-deficient Tregs expressed similar levels of Treg signature genes (*Foxp3*, *Tnfrsf18* encoding GITR, *Ikzf2*, *Il2ra*, *Capg*) and increased expression of key inflammatory cytokines (*Il1a*, *Il1b*, *Il4*, *Il6*, *Il17a*, *Il17f*) (Supplemental Figure 3D), which was similar to that of aged Tregs. Yet they were defective in suppressing Tconv cell proliferation with impaired expansion (Figure 4G) and reduced proliferative capacity (Supplemental Figure 3, E and F) and survival (Supplemental Figure 3G). Consistent with what was observed in *Cd4-Cre Dcaf1*$^{fl/fl}$ mice, *FGC Dcaf1*$^{fl/fl}$ Tregs also adopted an aging phenotype with elevated expression of senescence signature genes (Figure 4H), indicating a Treg-intrinsic role of DCAF1 in restraining Treg aging.

Treg aging co-opts inflammation to promote immunological aging. We noticed that Tconv cells in young *FGC Dcaf1*$^{fl/fl}$ mice acquired an aging phenotype (Figure 4H), although they expressed normal levels of DCAF1 (Supplemental Figure 3B). This result suggested that the aberrant inflammation resulted from Treg aging and functional deterioration could promote T cell aging through cell-extrinsic mechanisms. To test this, we generated mixed bone marrow chimeras in which *FGC Dcaf1*$^{fl/fl}$

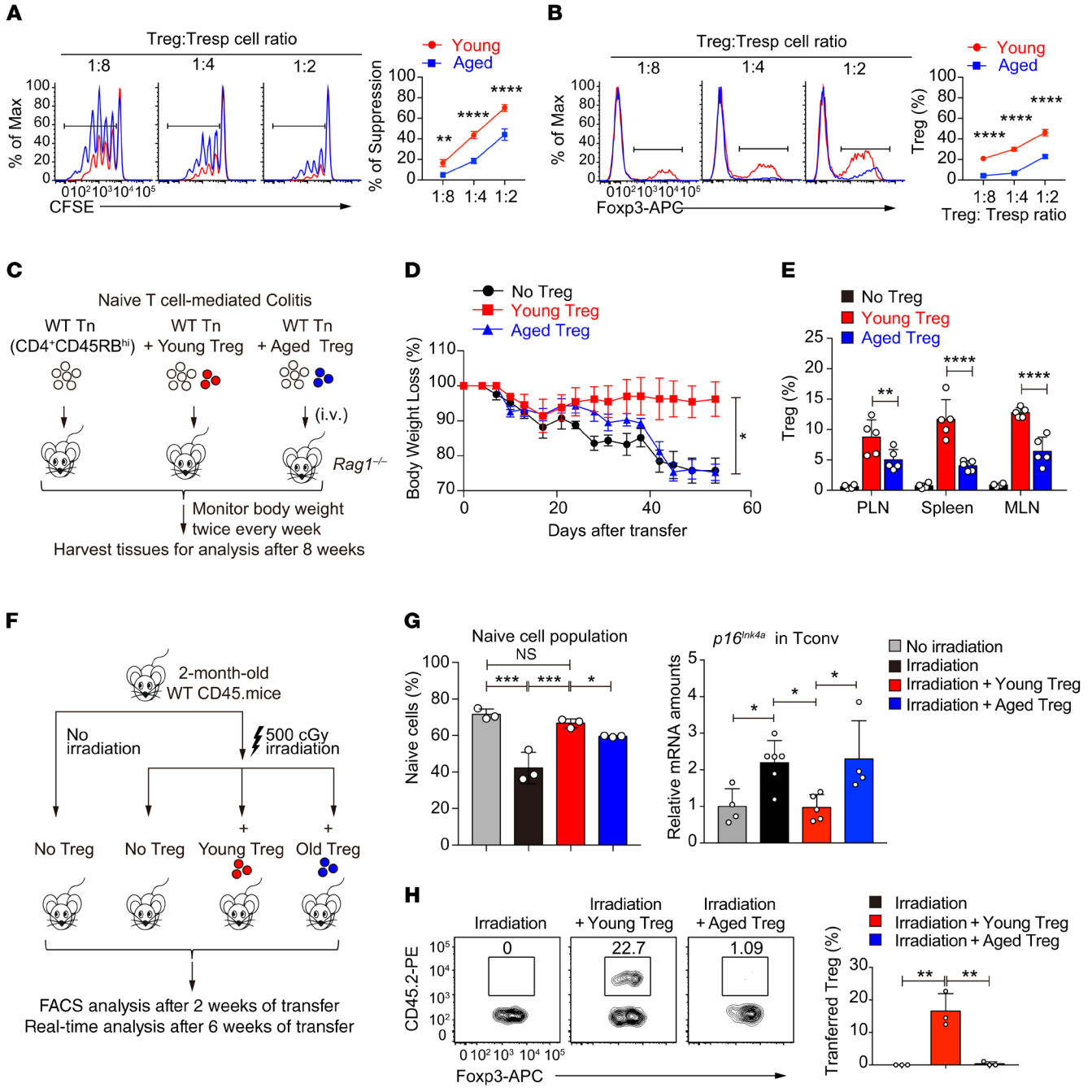

Figure 2. Deterioration of Treg function in aged mice. (**A** and **B**) Comparison of the suppressive activity of young and aged Tregs by in vitro suppression assays (**A**); the composition of Foxp3$^+$ Tregs was also assessed by flow cytometry (**B**) (n = 3 mice of 3 experiments; representative results are shown; means ± SD, $^{**}P < 0.01$, $^{****}P < 0.0001$, by 2-way ANOVA followed by Holm-Šidák multiple-comparisons test). Tresp cell, responder T cell. (**C**) Schematic diagram of T cell–induced colitis. *Rag1*$^{-/-}$ recipients received WT naive CD4$^+$CD45RB^{hi} T cells (Tn) alone or in combination with young or aged CD4$^+$CD25$^+$ Tregs. (**D**) After transfer, the body weight loss was monitored to examine the suppressive ability of young and old Tregs (n = 10 mice per group of 2 experiments; means ± SEM, $^*P < 0.05$ for young Tregs vs. no Tregs, $P = 0.3682$ for aged Tregs vs. no Tregs, $^*P < 0.05$ for young Tregs vs. aged Tregs, by 2-way-ANOVA followed by Holm-Šidák test). (**E**) Percentages of Tregs recovered in periphery lymph nodes (PLN), spleens, and mesenteric lymph nodes (MLN) in recipient mice at the end of the experiments (n = 5 mice of 2 experiments; means ± SD, $^{**}P < 0.01$, $^{****}P < 0.0001$, by 2-way ANOVA followed by Holm-Šidák multiple-comparisons test). (**F**) Schematic diagram of whole-body irradiation–induced senescence. WT CD45.1 mice were sublethally irradiated and transferred with or without young or aged CD4$^+$CD25$^+$ Tregs. (**G**) The naive T cell population (CD62L^{hi}CD44^{lo}CD45.1$^+$) (left) and *p16*^{Ink4a} mRNA expression (right) of host Tconv cells in the indicated group of mice were analyzed. (**H**) The percentage of transferred Tregs (CD45.2$^+$) among host Tregs in the recipient mice (CD45.1$^+$) was analyzed by flow cytometry (n = 3–5 mice of 3 experiments; means ± SD, $^*P < 0.05$, $^{**}P < 0.01$, $^{***}P < 0.001$, by 1-way ANOVA followed by Tukey's multiple-comparisons test).

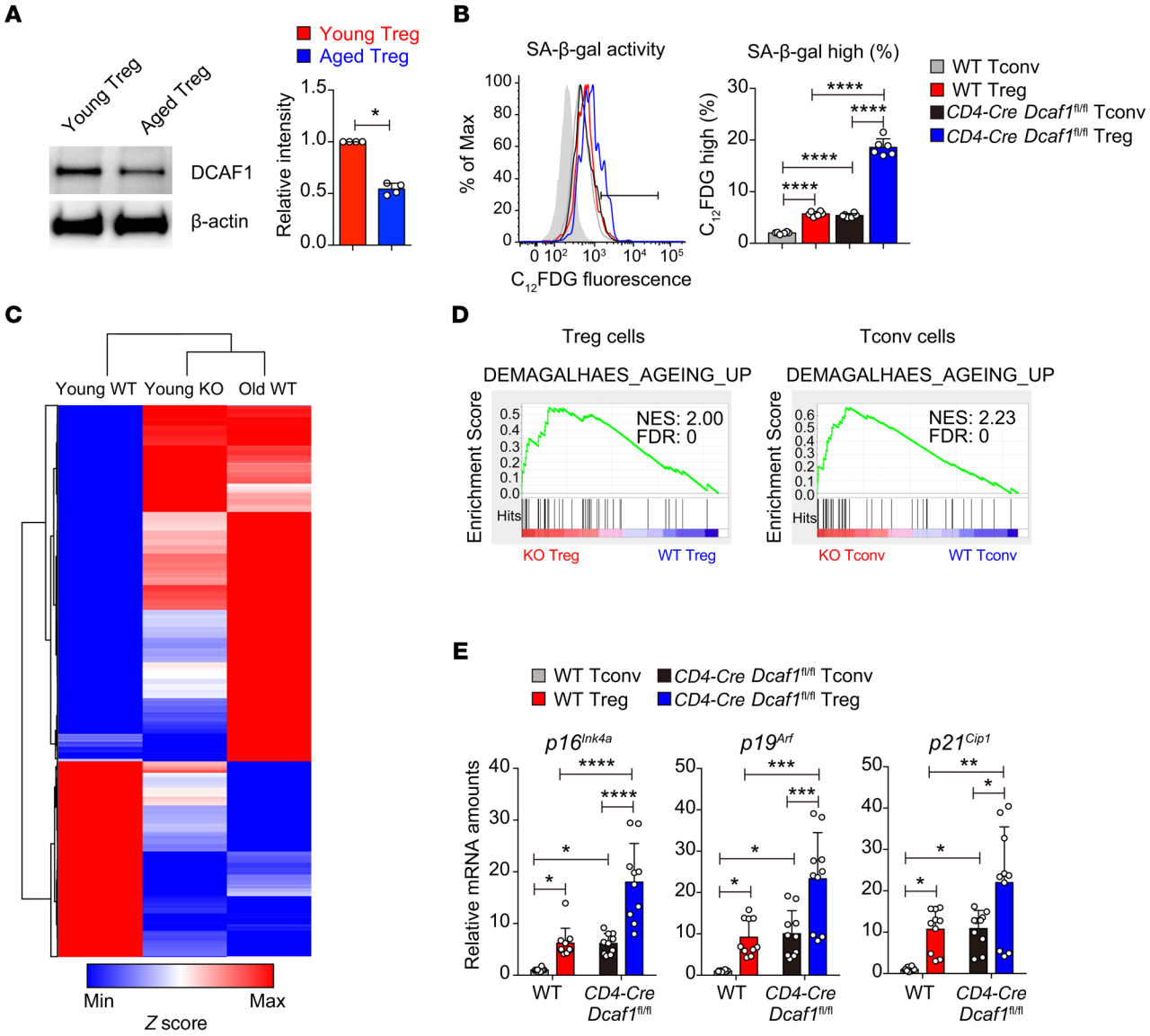

Figure 3. DCAF1 deletion leads to T cell aging in young mice. (**A**) Protein expression of DCAF1 in Tregs isolated from young and aged mice, assessed by immunoblotting. Left: Representative of 3 independent experiments. Right: Statistical summary, means ± SD, $^*P < 0.05$, by Mann-Whitney *U* test. (**B**) SA-β-gal activity in $CD4^+CD25^+$ Tregs and $CD4^+CD25^-$ Tconv cells in splenocytes from mice of indicated genotypes, analyzed by flow cytometry with the fluorescent β-gal substrate C_{12}FDG (gray area, no C_{12}FDG; $n = 6$ mice of 3 experiments; representative results are shown; means ± SD, $^{****}P < 0.0001$, by 1-way ANOVA followed by Tukey's multiple-comparisons test). (**C**) Heatmap analysis of RNA-Seq data sets to compare top regulated genes in young WT, young Dcaf1-deficient (KO), and aged WT Tregs. The depicted distance was calculated based on Pearson's correlation. (**D**) Upregulation of the aging program in Dcaf1-deficient (KO) Tregs (left) and Tconv cells (right), revealed by GSEA of RNA-Seq data sets. (**E**) Comparison of aging signature gene expression in indicated T cells by qRT-PCR analysis of indicated genes ($n = 10$ mice of 4 experiments; means ± SD, $^*P < 0.05$, $^{**}P < 0.01$, $^{***}P < 0.001$, $^{****}P < 0.0001$, by 1-way ANOVA followed by Tukey's multiple-comparisons test).

and *FGC Dcaf1*$^{fl/+}$ T cells coexisted in the same hosts (Figure 5A). The presence of Dcaf1-sufficient Tregs in mixed bone marrow chimeras suppressed T cell activation and cytokine production (Figure 5, B–E) and prevented Tconv cells from acquiring aging phenotype (Figure 5F). Nonetheless, the aging phenotype of Dcaf1-deficient Tregs persisted (Figure 5F). Consistently, Dcaf1-deficient Tregs remained inferior in populating the periphery as compared with the coexisting WT Tregs in the mixed bone marrow chimeras (Figure 5G). Taken together with the results in Figure 4, these findings not only reaffirm a critical role for DCAF1 in restraining Treg aging, but also suggest that Treg aging and function deterioration may cause uncontrolled Tconv cell activation, inflammation, and immunological aging.

DCAF1 is required to restrain the aging of human T cells. While it has been documented that T cells and Tregs in HIV patients display premature aging phenotypes (35, 36, 38, 39), the molecular mechanisms remain to be elucidated. To investigate whether DCAF1 is critical to prevent human T cell aging, we used *Dcaf1* shRNA lentivirus to knock down DCAF1 expression and examined the aging phenotypes in human T cells. We designed 2 different shRNA constructs to efficiently downregulate DCAF1 expression in human T cells (Figure 6A). We found that shRNA-mediated DCAF1 knock-

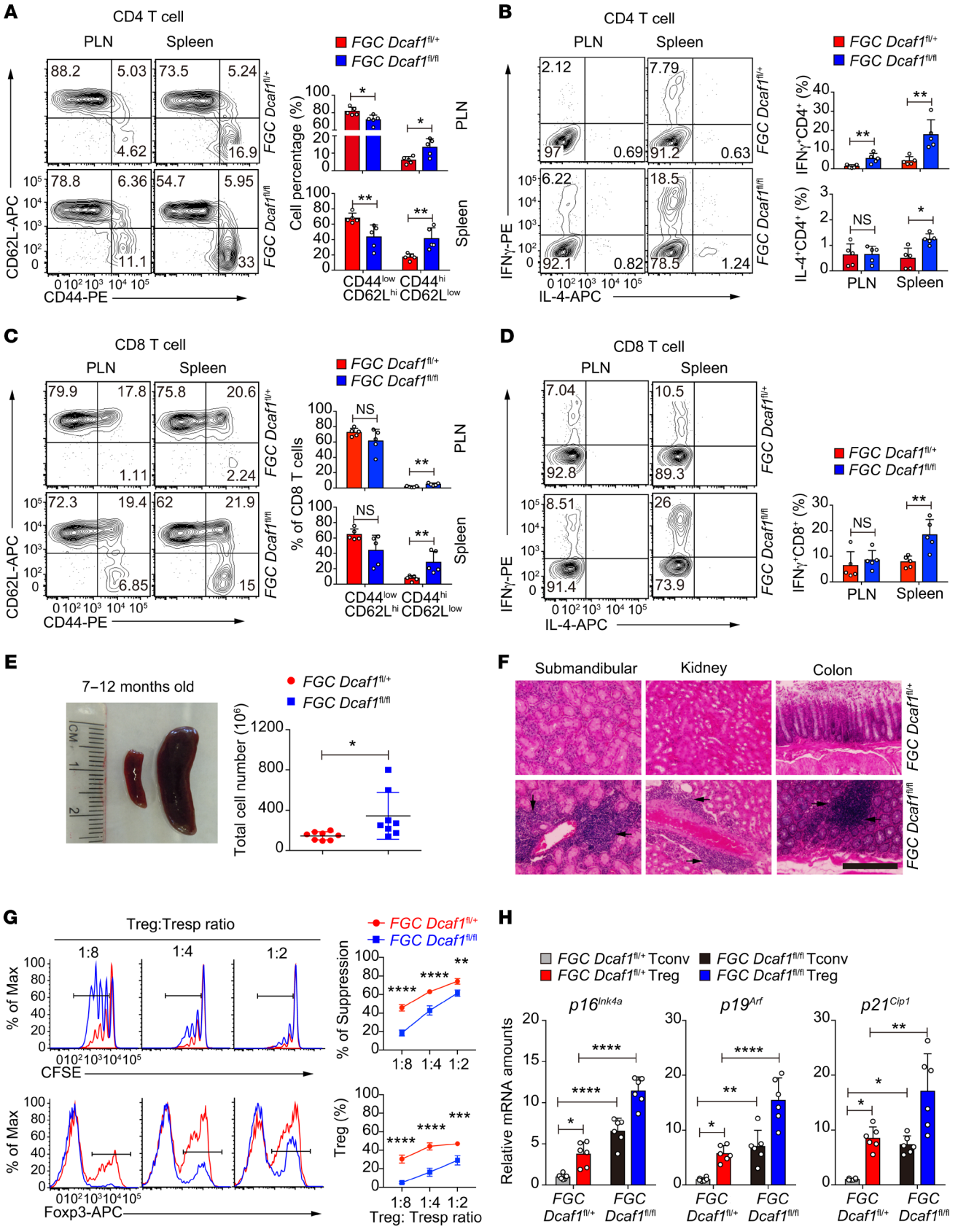
A
CD4 T cell
PLN
Spleen
FGC Dcaf1fl/+
FGC Dcaf1fl/fl
88.2
5.03
4.62
73.5
5.24
16.9
78.8
6.36
11.1
54.7
5.95
33
CD62L-APC
CD44-PE
Cell percentage (%)
CD44low CD62Lhi
CD44hi CD62Llow
B
CD4 T cell
2.12
7.79
97
0.69
91.2
0.63
6.22
18.5
92.1
0.82
78.5
1.24
IFNγ-PE
IL-4-APC
IFNγ+CD4+ (%)
IL-4+CD4+ (%)
NS
C
CD8 T cell
79.9
17.8
1.11
75.8
20.6
2.24
72.3
19.4
6.85
62
21.9
15
% of CD8 T cells
D
CD8 T cell
7.04
10.5
92.8
89.3
8.51
26
91.4
73.9
IFNγ+CD8+ (%)
E
7–12 months old
Total cell number (10^6)
F
Submandibular
Kidney
Colon
G
Treg:Tresp ratio
1:8
1:4
1:2
% of Max
CFSE
Foxp3-APC
% of Suppression
Treg (%)
Treg: Tresp ratio
H
FGC Dcaf1fl/+ Tconv
FGC Dcaf1fl/+ Treg
FGC Dcaf1fl/fl Tconv
FGC Dcaf1fl/fl Treg
p16Ink4a
p19Arf
p21Cip1
Relative mRNA amounts

Figure 4. DCAF1 is required to prevent Treg aging and inflammaging. (**A** and **B**) Distribution of naive and effector memory CD4$^+$ T cells (**A**) and IFN-γ and IL-4 production of CD4$^+$ T cells (**B**) in peripheral lymph nodes (PLN) and spleens of 2-month-old mice of indicated genotypes, assessed by flow cytometry (n = 5 mice, 5 experiments; representative results shown; means ± SD, $^*P < 0.05$, $^{**}P < 0.01$, Mann-Whitney U test). (**C** and **D**) Distribution of naive and effector memory CD8$^+$ T cells (**C**) and IFN-γ and IL-4 production of CD8$^+$ T cells (**D**) in peripheral lymph nodes and spleens of 2-month-old mice of indicated genotypes, assessed by flow cytometry (n = 5 mice, 5 experiments; representative results shown; means ± SD, $^{**}P < 0.01$, Mann-Whitney U test). (**E**) Splenomegaly (left) and increased splenocyte counts (right) in 7- to 12-month-old *FGC Dcaf1*$^{fl/fl}$ mice (n = 8 mice, 8 experiments; representative results shown, means ± SD, $^*P < 0.05$, 2-sided t test). (**F**) Histology to compare lymphocytic infiltration in the submandibular gland, kidney, and colon in 7- to 12-month-old littermates of indicated genotypes (scale bar: 100 μm; arrows indicate lymphocyte infiltration foci; results are representative of 5 mice). (**G**) Comparison of the suppressive activity of Tregs of indicated genotype by in vitro suppression assays (top); the composition of Foxp3$^+$ Tregs was also assessed by flow cytometry (bottom) (n = 3 mice, 3 experiments; representative results shown; means ± SD, $^{**}P < 0.01$, $^{***}P < 0.001$, $^{****}P < 0.0001$, 2-way ANOVA followed by Holm-Šidák multiple-comparisons test). (**H**) Comparison of aging signature gene expression in Tregs and Tconv cells from mice of indicated genotypes, assessed by qRT-PCR analysis of indicated genes (n = 6 mice, 6 experiments; means ± SD, $^*P < 0.05$, $^{**}P < 0.01$, $^{****}P < 0.0001$, 1-way ANOVA followed by Tukey's multiple-comparisons test).

down led to increased ROS level (Figure 6B), increased SA-β-gal activity in human T cells (Figure 6C), and increased expression of aging-related genes including *p16^{Ink4a}* (Figure 6D). Therefore, DCAF1 is important to prevent human T cell aging, indicating that HIV infection may cause the premature aging of human T cells by interfering with DCAF1.

DCAF1 is required to suppress aberrant ERK activation during aging. Intrigued by the above-mentioned findings, we further investigated the molecular mechanisms underlying Treg aging. We found that both aged Tregs (Supplemental Figure 4A) and young Dcaf1-deficient Tregs (Supplemental Figure 4B) paradoxically had a drastic ERK activation that normally promotes cell proliferation (40), despite their poor proliferative capacity. Such an ERK activation was not due to enhanced IL-2 signaling, because IL-2–activated STAT5 was reduced in these Tregs (Supplemental Figure 4, C and D). The activation of ERK–Jun–p38 MAPK was reported in aged T cells from old humans (>65 years) and mice (16–20 months old) (41). Yet the upstream stimuli remain unclearly defined. Using tamoxifen-inducible-Cre (*ER-Cre*) mice (42), we were able to delete DCAF1 in *ER-Cre Dcaf1*$^{fl/fl}$ T cells acutely upon 4-hydroxy-tamoxifen treatment and analyze the causal effect of acute DCAF1 deletion. We found that DCAF1 was critical to restrict such ERK activation because acute deletion of DCAF1 in activated T cells led to ERK activation (Supplemental Figure 4E) and upregulation of the critical aging gene *p16^{Ink4a}* (Supplemental Figure 4F). Importantly, interfering with ERK activation attenuated the upregulation of *p16^{Ink4a}* in Dcaf1-deficient T cells (Supplemental Figure 4, G and H). Thus, the observed ERK activation is important to promote T cell aging (43) in a DCAF1-dependent manner.

DCAF1 controls ROS accumulation, ERK activation, and Treg aging through GSTP1. We next explored the pathways contributing to aberrant ERK activation and aging in aged and Dcaf1-deficient Tregs. Unbiased genome-wide RNA-Seq analysis revealed that the ROS pathway, which is known to cause ERK activation, was upregulated and enriched in both aged Tregs and young Dcaf1-deficient Tregs (Figure 7, A and B). Although an appropriate level of ROS is important for T cell function (44), excessive ROS is a predominant contributor of cellular senescence and aging (45, 46). We found that the ROS level was significantly elevated in both aged and Dcaf1-deficient Tregs and Tconv cells (Figure 7, C and D). Additionally, acute deletion of DCAF1 in *ER-Cre Dcaf1*$^{fl/fl}$ T cells led to a prompt ROS upregulation in T cells (Figure 7E), preceding ERK activation (Supplemental Figure 4E) and upregulation of the aging signature gene *p16^{Ink4a}* (Supplemental Figure 4F). These results suggest that the excessive ROS contributed to ERK activation and aging in both aged and Dcaf1-deficient Tregs.

To study how DCAF1 regulates ROS, we analyzed the DCAF1 interactome from 2 independent immunoprecipitation–mass spectrometry (IP-MS) experiments using both T and non-T cells (34, 47). While DCAF1-regulated pathways, including DNA repair, cell cycle arrest, and unfolded protein response, could indirectly induce ROS (Supplemental Figure 5, A and B), DCAF1 was found bound to GSTP1, which was further validated both by coimmunoprecipitation assays in 293T cells and by endogenous immunoprecipitation in mouse T cells (Figure 7, F and G). GSTP1 is one of the glutathione-*S*-transferase (GST) family members that catalyze intracellular detoxification reactions by conjugating glutathione (GSH) with hydrophobic and electrophilic compounds (48). Depletion of Gstp1 or pharmacological inhibition of its activity increases ROS level and ERK phosphorylation (49). Overexpression of Gstp2 (a Gstp1 ortholog in *Caenorhabditis elegans*) enhanced stress resistance and extended lifespan in *C. elegans* (50). Given the known function of DCAF1 as a component of an E3 ubiquitin ligase complex to not only regulate protein degradation via polyubiquitylation but also regulate protein function via monoubiquitylation (47), we investigated whether DCAF1 regulated the ubiquitylation of GSTP1. We found that GSTP1 was monoubiquitylated and DCAF1 promoted monoubiquitylation but not polyubiquitylation of GSTP1 (Supplemental Figure 5C). This suggests that DCAF1 may facilitate GSTP1 function. Indeed, we found that expression of GSTP1 promoted GST activity and coexpression of DCAF1 further enhanced GST activity (Figure 7H). In agreement, GST activity was significantly downregulated in both aged and Dcaf1-deficient Tregs (Supplemental Figure 5, D and E). Additionally, knockdown of DCAF1 in human T cells led to decreased GST activity (Supplemental Figure 5F). Next, we overexpressed GSTP1 in Dcaf1-deficient T cells and found that overexpression of Gstp1 suppressed the excessive ROS accumulation (Figure 7I) and ERK phosphorylation (Supplemental Figure 6A) in Dcaf1-deficient T cells. Importantly, overexpression of GSTP1 corrected the proliferation defects of aged Tregs (Figure 7J). These findings suggest that DCAF1 promotes the function of GSTP1 via monoubiquitylation to restrain ROS accumulation and Treg aging.

Suppression of ROS reinvigorates the proliferation and function of aged Tregs. Multiple strategies have been developed to delay and even reverse the aging process (9). As ROS are a predominant contributor of cellular senescence and aging (45, 46), we next wondered whether targeting excessive ROS could suppress Treg aging and rejuvenate the suppressive function of aged Tregs. By

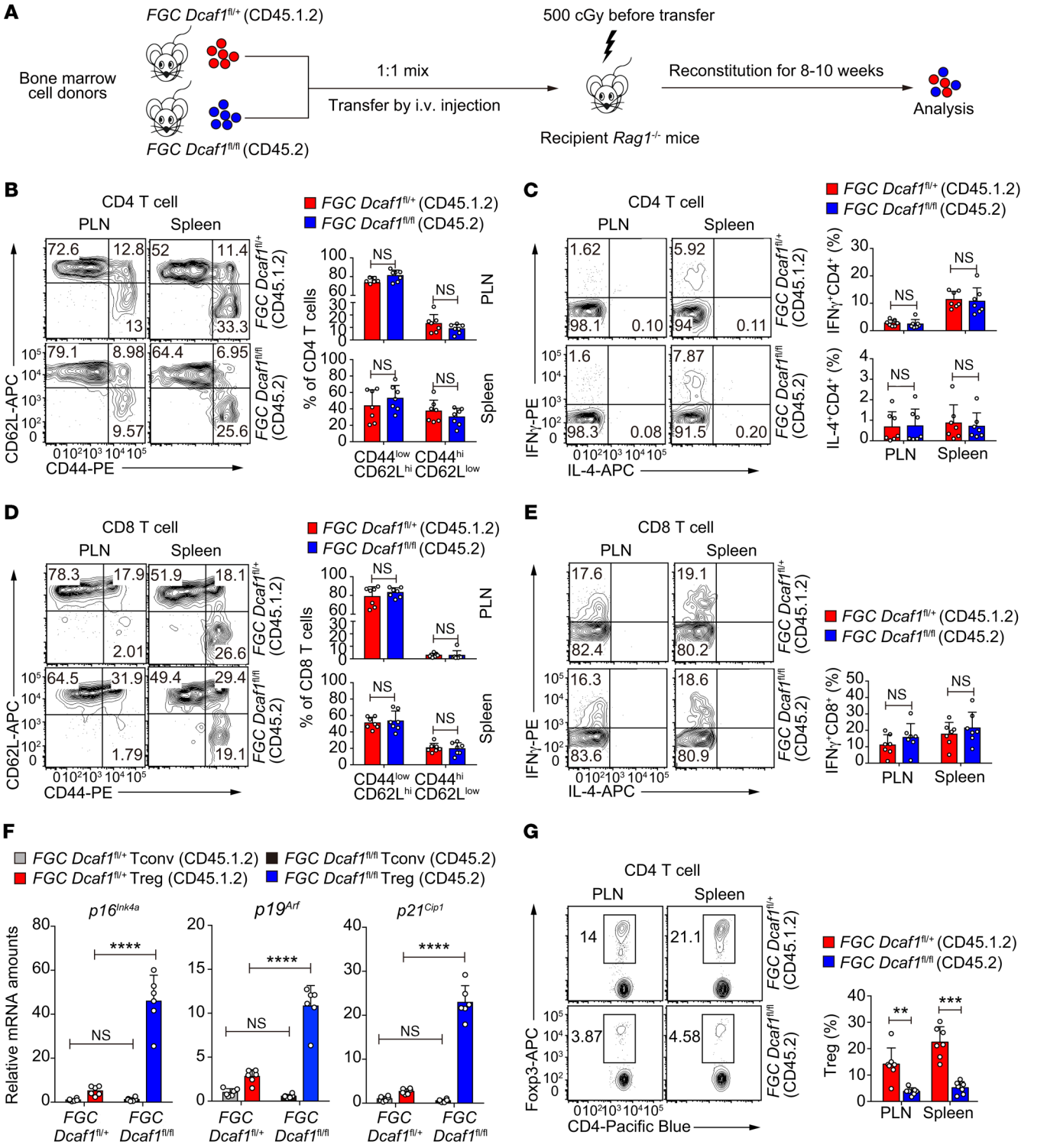

Figure 5. Dcaf1-deficient Tregs co-opt inflammation to promote the aging of Tconv cells. (**A**) Schematic diagram of the generation of mixed bone marrow chimeric mice to contain both *FGC Dcaf1*$^{fl/+}$ (CD45.1.2) and *FGC Dcaf1*$^{fl/fl}$ (CD45.2) T cells. (**B**–**E**) Flow cytometry of CD44/CD62L expression (**B**) and cytokine production (**C**) by CD4$^+$ T cells of indicated genotypes, and of CD44/CD62L expression (**D**) and cytokine production (**E**) by CD8$^+$ T cells of indicated genotypes, in peripheral lymph nodes (PLN) and spleens of mixed bone marrow chimeric mice generated as described in **A** (n = 7 mice of 7 experiments; representative results are shown; means ± SD, by Mann-Whitney U test). (**F**) Comparison of aging signature gene expression in Tregs and Tconv cells of indicated genotypes in mixed bone marrow chimeric mice generated as described in **A** (n = 6 mice of 3 experiments; means ± SD, $^{****}P < 0.0001$, by 1-way ANOVA followed by Tukey's multiple-comparisons test). (**G**) Flow cytometry of Tregs of indicated genotypes in peripheral lymph nodes and spleens of mixed bone marrow chimeric mice generated as described in **A** (n = 7 mice of 7 experiments; representative results are shown; means ± SD, $^{**}P < 0.01$, $^{***}P < 0.001$, by Mann-Whitney U test).

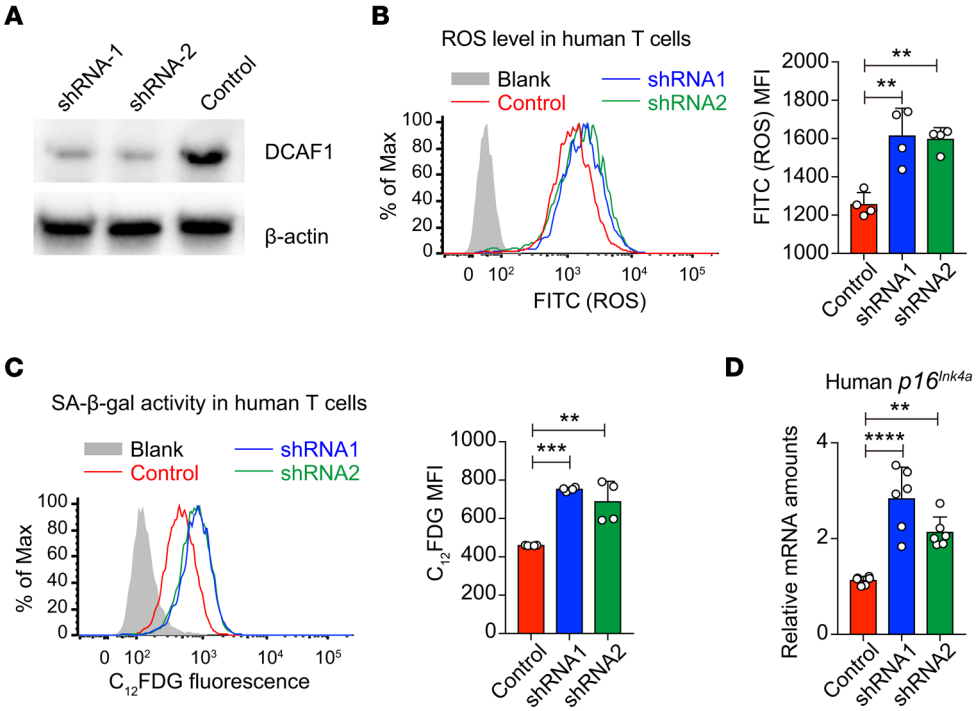

Figure 6. DCAF1 is required to prevent human T cell aging. (**A**) The protein expression of DCAF1 and β-actin in human 293T cells transduced with lentivirus expressing 2 shRNAs targeting *Dcaf1* and scrambled control for 4 days. The results are representative of 3 independent experiments. (**B**) Flow cytometry of ROS level in human T cells transduced with lentivirus expressing 2 shRNAs targeting *Dcaf1* and scrambled control for 4 days, analyzed by 2′,7′-dichlorofluorescin diacetate (DCFDA) (gray area, no DCFDA; $n = 4$; representative results of 2 independent experiments are shown; means ± SD, $^{**}P < 0.01$, by 1-way ANOVA followed by Tukey's multiple-comparisons test). (**C**) SA-β-gal activity in human T cells transduced with lentivirus expressing 2 shRNAs targeting *Dcaf1* and scrambled control for 6 days, assessed by flow cytometry with the fluorescent β-gal substrate C_{12}FDG (gray area, no C_{12}FDG; $n = 4$; representative flow cytometry results are shown; means ± SD, $^{**}P < 0.01$, $^{***}P < 0.001$, by 1-way ANOVA followed by Tukey's multiple-comparisons test). (**D**) qRT-PCR analysis to determine mRNA expression of *p16*^{Ink4a} in human T cells transduced with 2 shRNAs targeting *Dcaf1* and scrambled control for 6 days ($n = 6$ from 2 independent experiments; means ± SD, $^{**}P < 0.01$, $^{****}P < 0.0001$, by 1-way ANOVA followed by Tukey's multiple-comparisons test).

using ROS scavengers including *N*-acetyl-L-cysteine (NAC) and GSH, we effectively downregulated ROS level in both aged and Dcaf1-deficient Tregs (Figure 8, A and B). Interestingly, suppression of excessive ROS also drastically promoted the proliferation of both aged and Dcaf1-deficient Tregs (Figure 8, C and D). Next we analyzed the effect of ROS scavengers on the function of aged and Dcaf1-deficient Tregs by in vitro suppression assay. To avoid the effects of NAC/GSH on responder T cells, we pretreated Tregs with NAC and GSH for 24 hours before adding them into coculture for Treg suppression assay. We found that ROS scavenger treatment was effective in reinvigorating the immune suppression function of aged and Dcaf1-deficient Tregs (Figure 8, E and F). Taken together, these findings demonstrate that excessive ROS is a critical mechanism underlying Treg aging and functional deterioration during immunological aging.

Discussion

Aging and age-associated diseases have become pressing health issues worldwide (2). The immune system is greatly affected by aging, displaying chronic inflammation (inflammaging) and reduced immune function (immunosenescence). Thus, understanding the cellular and molecular mechanisms underlying the alterations of immune regulation during aging is vital in order to find ways to address age-related health issues. This study investigated whether and how the function of Tregs is regulated during immunological aging. By combining comprehensive in vitro and in vivo approaches, we showed an unexpected cell-intrinsic propensity of Tregs to preferentially senesce over Tconv cells through DCAF1/GSTP1/ROS–dependent mechanisms, causing an increasing imbalance between the function of Tregs and Tconv cells during aging to favor Tconv cell activation and inflammation, which in turn further promotes immunological aging (Supplemental Figure 7). Our findings support the notion that Tregs play critical roles in restraining immunological aging and offer potential molecular targets, such as the GSTP1/ROS axis, for reinvigorating Treg function during aging.

The Treg population has consistently been found to be elevated in lymphoid tissues during immunological aging in both human and mouse studies (18, 20, 23). It is intuitive to believe that such a Treg increase leads to increased immune suppression. Early studies suggested that the function of aged Tregs was unchanged or increased based on in vitro experiments using bulk T cells without specifically investigating the intrinsic function of Tregs (17–19). While these findings appear to explain certain age-related conditions, including higher incidence of tumor development, which could also be driven by aging-related chronic inflammation (51), they contradict the observation that immunological aging is marked by a low-grade, chronic systemic inflammation with

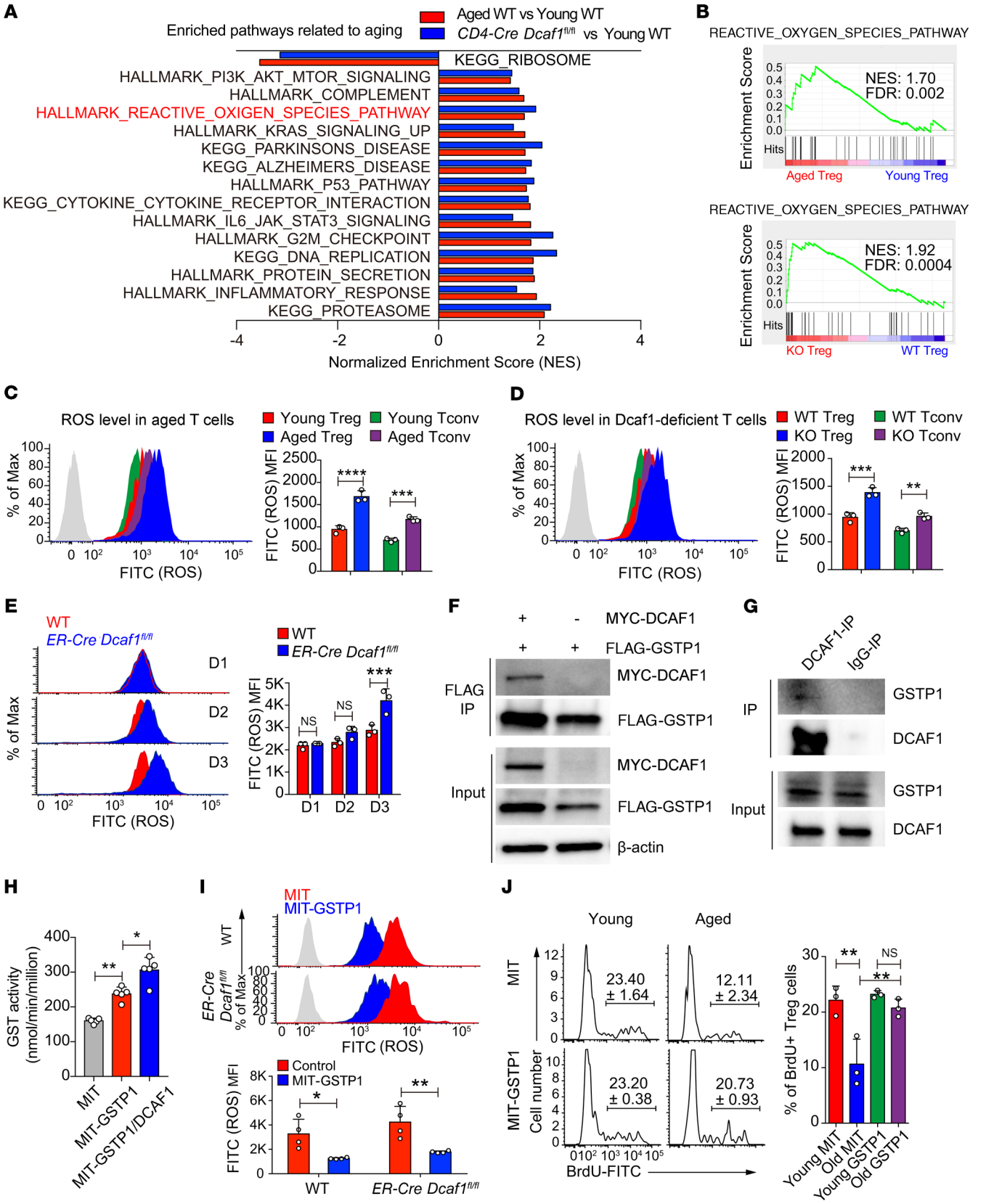
A
Enriched pathways related to aging
Aged WT vs Young WT
CD4-Cre Dcaf1fl/fl vs Young WT
KEGG_RIBOSOME
HALLMARK_PI3K_AKT_MTOR_SIGNALING
HALLMARK_COMPLEMENT
HALLMARK_REACTIVE_OXIGEN_SPECIES_PATHWAY
HALLMARK_KRAS_SIGNALING_UP
KEGG_PARKINSONS_DISEASE
KEGG_ALZHEIMERS_DISEASE
HALLMARK_P53_PATHWAY
KEGG_CYTOKINE_CYTOKINE_RECEPTOR_INTERACTION
HALLMARK_IL6_JAK_STAT3_SIGNALING
HALLMARK_G2M_CHECKPOINT
KEGG_DNA_REPLICATION
HALLMARK_PROTEIN_SECRETION
HALLMARK_INFLAMMATORY_RESPONSE
KEGG_PROTEASOME
-4 -2 0 2 4
Normalized Enrichment Score (NES)
B
REACTIVE_OXYGEN_SPECIES_PATHWAY
Enrichment Score
NES: 1.70
FDR: 0.002
Hits
Aged Treg
Young Treg
REACTIVE_OXYGEN_SPECIES_PATHWAY
Enrichment Score
NES: 1.92
FDR: 0.0004
Hits
KO Treg
WT Treg
C
ROS level in aged T cells
Young Treg
Young Tconv
Aged Treg
Aged Tconv
% of Max
FITC (ROS)
FITC (ROS) MFI
****
***
D
ROS level in Dcaf1-deficient T cells
WT Treg
WT Tconv
KO Treg
KO Tconv
% of Max
FITC (ROS)
FITC (ROS) MFI
***
**
E
WT
ER-Cre Dcaf1fl/fl
D1
D2
D3
% of Max
FITC (ROS)
FITC (ROS) MFI
NS
NS
***
F
MYC-DCAF1
FLAG-GSTP1
FLAG IP
Input
β-actin
G
DCAF1-IP
IgG-IP
IP
Input
GSTP1
DCAF1
H
GST activity (nmol/min/million)
**
*
MIT
MIT-GSTP1
MIT-GSTP1/DCAF1
I
MIT
MIT-GSTP1
WT
ER-Cre Dcaf1fl/fl
% of Max
FITC (ROS)
Control
MIT-GSTP1
FITC (ROS) MFI
*
**
J
Young
Aged
MIT
MIT-GSTP1
Cell number
23.40 ± 1.64
12.11 ± 2.34
23.20 ± 0.38
20.73 ± 0.93
BrdU-FITC
% of BrdU+ Treg cells
**
NS
**
Young MIT
Old MIT
Young GSTP1
Old GSTP1

Figure 7. DCAF1 is required to suppress ROS in Tregs. (**A**) Pathways commonly enriched in aged and Dcaf1-deficient (*CD4-Cre Dcaf1*$^{fl/fl}$) Tregs based on GSEA of RNA-Seq data sets (FDR < 0.05). (**B**) Enrichment of ROS pathway in aged versus young WT Tregs (top) and Dcaf1-deficient (KO) versus WT Tregs (bottom) by GSEA of RNA-Seq data sets. (**C**–**E**) Flow cytometry of ROS level in indicated T cell populations from young WT and aged WT mice (**C**), young *Dcaf1*-deficient mice (**D**) and activated WT and *ER-Cre Dcaf1*$^{fl/fl}$ CD4$^+$ T cells treated with 4-hydroxy-tamoxifen for indicated days (**E**), analyzed by DCFDA (gray area, no DCFDA; n = 3 mice of 3 experiments; representative results are shown; means ± SD, $^{**}P < 0.01$, $^{***}P < 0.001$, $^{****}P < 0.0001$, by 2-way ANOVA followed by Holm-Šidák multiple-comparisons test). (**F** and **G**) Interaction of GSTP1 and DCAF1 by coimmunoprecipitation in 293T cells (**F**) and by endogenous immunoprecipitation using anti-DCAF1 antibody in mouse T cells (**G**). The results are representative of 3 independent experiments. (**H**) GST activity in 293T cells after overexpression of GSTP1 and DCAF1 for 4 days; n = 5; means ± SD, $^{*}P < 0.05$, $^{**}P < 0.01$, by Mann-Whitney U test. (**I**) Flow cytometry of ROS level in activated WT and *ER-Cre Dcaf1*$^{fl/fl}$ CD4$^+$ T cells transduced with MIT (MSCV-IRES-Thy1.1) or MIT-GSTP1 virus in the presence of 4-hydroxy-tamoxifen, analyzed by DCFDA (gray area, no DCFDA; n = 3–4 experiments; means ± SD, $^{*}P < 0.01$, $^{**}P < 0.05$, by 2-way ANOVA followed by Holm-Šidák multiple-comparisons test). (**J**) Proliferation assayed by BrdU incorporation in young and aged Tregs transduced with MIT or MIT-Gstp1 virus (n = 3 experiments; means ± SD, $^{**}P < 0.01$, by 1-way ANOVA followed by Tukey's multiple-comparisons test).

accumulation of effector memory T cells and is also associated with a high incidence of autoimmunity (52). Moreover, emerging evidence indicates that aged Tregs may be functionally defective in vivo (20, 21). The discrepancy could be due to the difference in the assays used. In the studies using ^{3}H-thymidine incorporation assay to assess Treg suppression, the proliferative capacity of responder T cells and Tregs could not be distinguished. Therefore a decrease in ^{3}H-thymidine could be due to reduced proliferation of responder T cells, Tregs, or both. Thus, the results of ^{3}H-thymidine incorporation assay are not only determined by responder T cell proliferation, but also confounded by coexisting Tregs. Therefore, the results of Treg suppression assayed by ^{3}H-thymidine incorporation may vary substantially, and conflicting results of how well aged Tregs suppress are indeed reported (20, 27). To specifically assess the proliferation of Tregs and responder T cells, we distinguished them by their expression of different congenic markers (CD45.1 vs. CD45.2). Using this method, we found that young Tregs proliferated substantially to contribute to ^{3}H-thymidine incorporation of total cell culture. Yet aged Tregs proliferated much less, which may contribute to the reduced ^{3}H-thymidine incorporation of total cell culture. Taken together with results from the colitis model and irradiation-induced aging model, our study demonstrated that aged Tregs manifested exacerbated aging to contribute to deteriorated proliferation in response to activation in vitro and in vivo and were inferior in suppressing Tconv cell activation during aging. These findings therefore shed light on the long-sought mechanisms underlying age-associated chronic inflammation that contributes to age-related morbidities.

Accelerated T cell senescence is found in patients with AIDS even after antiretroviral therapy (35, 36) and contributes to the high mortality rate that exists among patients with AIDS even when active HIV infection is under control (53). We found that DCAF1, an HIV-1 cellular target that is downregulated during aging, was essential to restrain T cell, especially Treg, aging. In addition, inflammation resulting from defective Treg function promoted T cell aging. These findings suggest that HIV may promote T cell attrition in patients with AIDS through 2 mutually related mechanisms. One is to target DCAF1 to directly induce T cell aging. The other is to trigger Treg aging to induce chronic inflammation, which in turn exacerbates the aging program of T cells for reduced function. This presents the interesting possibility that, by restoring DCAF1 function and reinvigorating Treg function, we may reduce systemic inflammation and T cell attrition to benefit patients with AIDS. Therefore, further study of the underlying mechanisms of DCAF1 downregulation during aging will not only benefit aging-related diseases but also provide a potential means to reduce immune senescence in patients with AIDS.

The cellular level of ROS is subject to tight redox regulation, and disruption of the ROS balance may lead to excessive ROS causing cellular senescence and aging (45, 46). Here we found that ROS level was preferentially increased in Tregs compared with Tconv cells regardless of age, which agrees with the previous finding that ROS is required for the suppressive function of Tregs (54). We found that excessive ROS impaired the proliferative capacity and function of aged Tregs, and ROS scavenging agents reinvigorated the proliferation and suppressive function of aged T cells. By using IP-MS–based DCAF1 interactome analysis, we identified one of the potential mechanisms, where DCAF1 regulated ROS through GSTP1-mediated ROS detoxification. Given the emerging role of GSH in buffering ROS and regulating multiple processes in T cells (55), further studies on the detailed mechanisms of the DCAF1/GSTP1 axis in regulating GSH-mediated detoxification pathway will provide valuable insights not only in immunological aging, but also in the general function of immune cells. Additionally, we found that many pathways regulating cellular ROS generation (56), including PI3K/Akt/mTOR, DNA damage/p53 response, and inflammation, were altered in aged Tregs. Therefore, both ROS generation and detoxification appear to be involved in controlling the function of aged Tregs. Interestingly, the inhibition of the mTOR signaling pathway has been associated with healthier aging and longevity, especially for the hematopoietic system (57), which suggests that PI3K/Akt/mTOR may be particularly important for Treg aging. It therefore warrants further investigation whether targeting mTOR may also ameliorate Treg aging and inflammation through reducing ROS. In addition, because the current study highlights a critical role for ROS in Treg aging, it proposes that targeting ROS may be a viable approach to rejuvenate Tregs to mitigate immunological aging. Therefore, further in-depth studies of ROS-related pathways that regulate Treg aging may shed new light on the precise mechanisms underlying immunological aging and reveal potential targets to mitigate the adverse effects of inflammaging with the aim of improving the health of the aging population.

Methods

Animals. *Rag1*$^{-/-}$, *Foxp3-GFP-Cre* (FGC), and CD45.1 congenic WT mice were purchased from The Jackson Laboratory and maintained on a C57BL/6 background. *Dcaf1*$^{fl/fl}$ (58), *Cd4-Cre* (59), and *ER-Cre* (42) mice were on a C57BL/6 background as reported previously. Aged WT

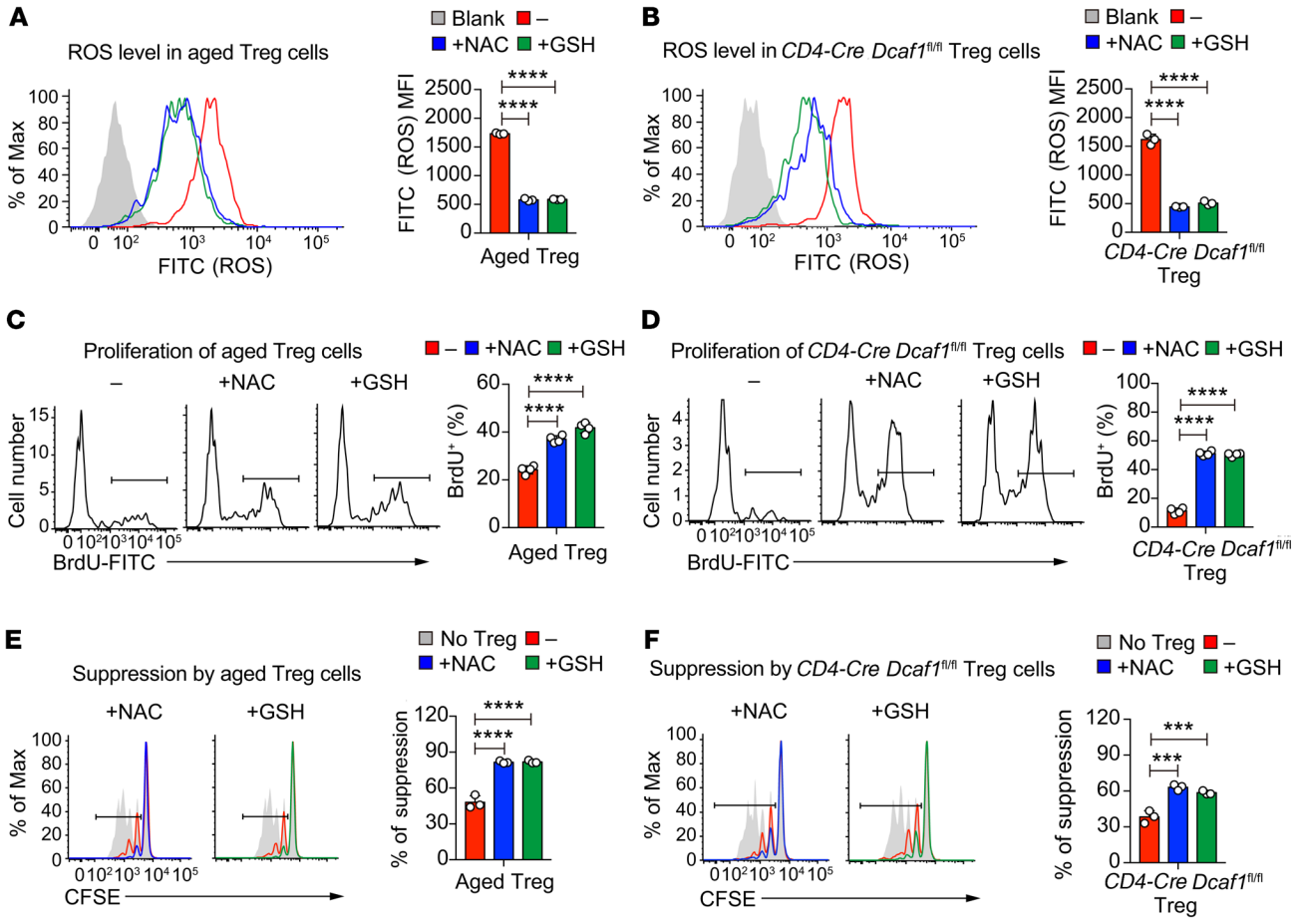

Figure 8. ROS is important for Treg aging and functional deterioration. (**A** and **B**) Flow cytometry of ROS levels in aged Tregs (**A**) and Dcaf1-deficient (*CD4-Cre Dcaf1*$^{fl/fl}$) Tregs (**B**) in the absence (–) or presence (+) of NAC (20 mM) or GSH (10 mM) (blank, no DCFDA; n = 3 mice of 3 experiments; representative results are shown; means ± SD, $^{****}P < 0.0001$, by 1-way ANOVA followed by Tukey's multiple-comparisons test). (**C**) Proliferation assayed by BrdU incorporation in aged Tregs in the absence (–) or presence (+) of NAC (20 mM) or GSH (10 mM) (n = 4 mice of 4 experiments; representative results are shown; means ± SD, $^{****}P < 0.0001$, by 1-way ANOVA followed by Tukey's multiple-comparisons test). (**D**) Proliferation assayed by BrdU incorporation in Dcaf1-deficient (*CD4-Cre Dcaf1*$^{fl/fl}$) Tregs in the absence (–) or presence (+) of NAC (20 mM) or GSH (10 mM) (n = 4 mice of 4 experiments; representative results are shown; means ± SD, $^{****}P < 0.0001$, by 1-way ANOVA followed by Tukey's multiple-comparisons test). (**E**) Suppressive activity of aged Tregs without (–) or with (+) pretreatment of NAC (20 mM) or GSH (10 mM), assessed by in vitro suppression assay (n = 3 mice of 3 experiments; representative results are shown; means ± SD, $^{****}P < 0.0001$, by 1-way ANOVA followed by Tukey's multiple-comparisons test). (**F**) Suppressive activity of Dcaf1-deficient (*CD4-Cre Dcaf1*$^{fl/fl}$) Tregs without (–) or with (+) pretreatment of NAC (20 mM) or GSH (10 mM), assessed by in vitro suppression assays (n = 3 mice of 3 experiments; representative results are shown; means ± SD, $^{***}P < 0.001$, by 1-way ANOVA followed by Tukey's multiple-comparisons test).

mice (>18 months old) were either from retired WT breeding mice or from the National Institute on Aging (NIA). All mice were housed and bred under specific pathogen–free conditions in the animal facility at the University of North Carolina at Chapel Hill.

Lymphocyte isolation, antibody staining, flow cytometry, and cell sorting. Lymphocytes were isolated from various lymphoid organs of mice of indicated ages and genotypes. Fluorescence-conjugated antibodies against CD4 (GK1.5), CD8 (53-6.7), CD45.1 (A20), CD45.2 (104), CD45RB (C363-16A), CD25 (PC61.5), CD44 (IM7), CD62L (MEL-14), IFN-γ (XMG1.2), and IL-4 (11B11) were purchased from BioLegend. The anti-Foxp3 antibody (FJK-16s) and Foxp3 staining kit (00-5523-00) were purchased from eBioscience, Thermo Fisher Scientific. Annexin V (BD Biosciences, 550474) and 7AAD (BD Biosciences, 559925) staining were used to assess apoptosis per the manufacturer's protocols. For intracellular cytokine staining, lymphocytes were stimulated for 4 hours with 50 ng/mL of PMA and 1 μM ionomycin in the presence of brefeldin A. The cells were stained with antibodies against surface markers and then fixed and permeabilized with a commercially available kit (BD Biosciences) for intracellular cytokine staining per the manufacturer's protocol. The stained cells were analyzed on an LSR-Fortessa station (BD Biosciences) or Canto (BD Biosciences).

For Treg sorting, CD25$^+$ T cells were first stained with anti-CD25 biotin antibody and enriched by Streptavidin MicroBeads (Miltenyi Biotec) and then stained with anti-CD4 and anti-CD25 fluorescence-conjugated antibodies. For CD4$^+$ T cell sorting, CD4$^+$ T cells were enriched by MACS beads (Miltenyi Biotec) and then stained with fluorescence-conjugated antibodies. Stained cells were washed and sorted on the Moflow cell sorter (Dako Cytomation, Beckman Coulter) by the flow facility of the University of North Carolina at Chapel Hill.

For detection of SA-β-gal activity in T cells with the fluorescent β-galactosidase substrate C_{12}FDG, the assay was adopted from a previously published protocol (60). Freshly isolated lymphocytes were

pretreated with 100 nM bafilomycin A1 (MilliporeSigma, B1793) for 1 hour before addition of 33 μM C_{12}FDG (MilliporeSigma, F2756) for an additional 2 hours in a 37°C incubator. The cells were harvested and washed in cold 1× PBS 3 times before staining with antibodies for FACS analysis.

For detection of ROS level in T cells, the DCFDA assay for detecting ROS was used as described previously (61). First, freshly isolated lymphocytes or cultured T cells were stained with antibodies. After staining, the cells were washed with 1× PBS and seeded in prewarmed medium in a 24-well plate. A final concentration of 2 μM DCFDA (MilliporeSigma, D6883) was added. Cells were cultured for 20 minutes and then harvested and washed with cold 1× PBS followed by flow cytometry. All the FACS data were analyzed with FlowJo software (Tree Star).

In vitro T cell culture, activation, and proliferation. To assess Treg proliferation in vitro, 1×10^4 Tregs from young mice (CD45.1) and 1×10^4 Tregs from aged mice (CD45.2) were cocultured with 1×10^5 naive $CD4^+$ T cells from young mice in the presence of soluble CD3 antibody (Bio X Cell, 2C11; 1 μg/mL) and 4×10^5 irradiated (3000 cGy) T cell–depleted splenocytes in RPMI 1640 medium containing 10% FBS, 1% penicillin-streptomycin, and 2.6 μL of β-mercaptoethanol. Cell proliferation was assessed by CFSE dilution assay or BrdU incorporation assay at indicated time points after activation.

For CFSE dilution assay, T cells were labeled in 2 μM CFSE (Life Technologies, C1157) and cultured in the presence of 2 ng/mL IL-2. For BrdU incorporation assay, cultured T cells were pulsed with BrdU for 1 hour before harvest, stained with BrdU staining kit per the manufacturer's protocols (BD Pharmingen, 559619), and analyzed by flow cytometry. To inhibit ERK phosphorylation, MEK inhibitor (PD98095) was added during T cell activation at a final concentration of 50 μM. For assays with ROS scavengers, a stock solution of 0.5 M NAC (MilliporeSigma, A9165) and 0.3 M GSH (VWR, IC10181405) was prepared in ddH_2O and adjusted to pH 7.0 with 10 N NaOH. A final concentration of 20 mM of NAC and 10 mM of GSH was added to cell culture.

In vitro Treg suppression assay. $CD4^+CD25^-CD62L^+CD44^-$ naive T cells (responder) from young WT mice (CD45.1) and $CD4^+CD25^+$ Tregs (suppressor) from young WT mice (CD45.2), aged WT mice (CD45.2), and young *FGC Dcaf1*$^{fl/fl}$ mice (CD45.2) were sorted by FACS.

To assess the efficacy of Treg-mediated immune suppression in vitro, 1×10^5 sorted responder T cells from young WT mice were labeled with CFSE and mixed with varying amounts (as indicated) of Treg suppressor cells. Cell mixtures were stimulated with soluble anti-CD3 (Bio X Cell, 2C11; 0.125 μg/mL) in the presence of 4×10^5 irradiated (3000 cGy) T cell–depleted splenocytes. The proliferation of responder cells was assessed by CFSE dilution detected by flow cytometry 72 hours after activation.

To assess the effect of ROS scavengers on Treg suppression, Tregs were pretreated with 20 mM of NAC or 10 mM of GSH for 24 hours in the presence of anti-CD3 (Bio X Cell, 2C11; 5 μg/mL) and anti-CD28 (Bio X Cell, 35.51; 2 μg/mL) antibodies and IL-2 (500 U/mL). Tregs were washed with RPMI 1640 medium to remove residual ROS scavengers before being used for in vitro suppression assay.

Human T cell purification, activation, and culture. For human T cell studies, $CD4^+$ T cells were purified by a human CD4 isolation kit (MACS, order 130-096-533) from human buffy coat obtained from Gulf Coast Regional Blood Center. Purified $CD4^+$ T cells were cultured in RPMI 1640 medium containing 10% FBS, 1% penicillin-streptomycin, and 2.6 μL of β-mercaptoethanol and activated with anti-CD3/CD28 stimulator (STEMCELL Technologies, catalog 10971) in the presence of human IL-2 (100 U/mL).

shRNA-mediated DCAF1 knockdown in human T cells. The human *Dcaf1* shRNA in lentivirus vector was from the RNAi Consortium, with shRNA1 (TRCN0000129831) targeting GCGCCAATAAACTTTACGTCA and shRNA2 (TRCN0000130734) targeting GCGCCAATAAACTTTACGTCA. HEK293T cells (ATCC) were transfected with 3 μg of shRNA plasmids and 3 μg of packaging plasmids (1 μg of psPAX2, 2 μg of pMD2.G) using FuGENE 6 (Promega) transfection reagent. After 48 hours, viruses were harvested, filtered through 0.45 μm syringe filters, and stocked in –80°C freezers.

For transduction of human T cells, human $CD4^+$ T cells were purified and activated with anti-CD3/anti-CD28 beads for 48 hours and then transduced with lentivirus encoding *Dcaf1* shRNA or scrambled control with 8 μg/mL polybrene (MilliporeSigma) by centrifuge at 1500 *g* for 120 minutes. Puromycin (2 μg/mL) was added for the selection of transduced cells after 48 hours of transduction. Cells were harvested 4 days after transduction for ROS analysis and 6 days after transduction for aging marker analysis.

Treg-mediated protection of naive $CD4^+$ T cell–elicited colitis in vivo. Sorted Tregs (1×10^5) from either young or aged mice (CD45.2) were mixed with 2×10^5 naive ($CD4^+CD25^-CD45RB^{hi}$) T cells sorted from young WT mice (CD45.1). The cell mixture was transferred into *Rag1*$^{-/-}$ mice. As a control, 2×10^5 naive $CD4^+$ T cells were transferred alone. To monitor colitis development, body weight of the recipient mice was measured weekly after the transfer. T cells from these mice were harvested and subjected to immunological analysis at the end of the experiments.

Generation of mixed bone marrow chimera. Bone marrow cells were isolated from age- and sex-matched *FGC Dcaf1*$^{fl/fl}$ (CD45.2) and *FGC Dcaf1*$^{fl/+}$ (CD45.1.2) littermates, mixed at a ratio of 1:1, and transferred into sublethally irradiated (500 cGy) *Rag1*$^{-/-}$ mice. T cells in the reconstituted recipients were analyzed 8–10 weeks after transfer.

Suppression of irradiation-induced Tconv cell aging by Tregs in vivo. The assays to induce T cell aging by irradiation were adopted from a previous publication (31). Young WT mice (CD45.1) were sublethally irradiated (400 cGy). A total of 2×10^6 Tregs isolated from either young or aged mice (CD45.2) were transferred into irradiated mice. At different time points after transfer, T cell populations in the irradiated mice with or without Treg transfer were analyzed.

RNA preparation, quantitative reverse transcriptase PCR, and RNA-Seq. Total RNA was prepared from T cells using TRIzol reagent (Invitrogen, Thermo Fisher Scientific) per the manufacturer's instructions and was reverse-transcribed into cDNA with iScript cDNA Synthesis Kit (Bio-Rad). Quantitative PCR was performed on an ABI 9700 real-time PCR system with TaqMan probe sets purchased from Applied Biosystems and Integrated DNA Technologies.

For the human T cell study, gene expression was analyzed by SYBR Green assay (Bio-Rad). The primers of *p16*^{Ink4a} (forward: CTCGTGCTGATGCTACTGAGGA; reverse: GGTCGGCGCAGTTGGGCTCC; catalog HP226191) and *β-actin* (forward: CACCATTGGCAATGAGCGGTTC; reverse: AGGTCTTTGCGGATGTCCACGT; catalog HP204660) were designed by OriGene.

For RNA-Seq analysis, total RNA was extracted from T cells using an RNeasy Mini kit (QIAGEN). RNA-Seq libraries were generated and poly(A)-enriched with 1 μg of RNA as input using the TruSeq RNA

Sample Prep Kit (Illumina). Indexed samples were sequenced using the 50 bp paired-end protocol with a HiSeq 2500 sequencing system (Illumina) per the manufacturer's protocol. Reads (30 million to 46 million reads per sample) were analyzed with Salmon software (version 0.9.1) (62) to align and quantify the transcript expression. R packages in Bioconductor, tximport, and tximportData (63) were used to aggregate transcript-level quantifications to the gene level, with the R package biomaRt for gene and transcript mapping.

The option "lengthScaledTPM" for countsFromAbundance in tximport was used to obtain the estimated counts at the gene level using abundance estimates scaled on the basis of the average transcript length over samples and the library size. For the differential expression (DE) analysis of RNA-Seq data, gene-level count matrix was passed into the DESeq2 package (64) as input directly from the tximport package. Based on the criteria $\log_2$(fold change) > 1.5 and adjusted P value < 0.05, 863 genes were differentially regulated in old Tregs compared with their young counterparts. The normalized gene expression data were retrieved from DESeq2 analysis after regulated log (rlog) transformation ("rlog" in DESeq2) (64). The Z score at gene-level average of normalized expression matrix was used to generate a heatmap in GENE-E (Broad Institute; https://software.broadinstitute.org/GENE-E).

Gene Set Enrichment Analysis (65) was performed using the Java application available from the Broad Institute (https://www.gsea-msigdb.org/gsea/datasets.jsp). Gene set databases including Hallmarks (h.all.v6.1.symbols.gmt) and the Kyoto Encyclopedia of Genes and Genomes (KEGG; c2.cp.kegg.v6.1.symbols.gmt) from the Molecular Signatures Database (MSigDB) (66) were used in the analysis. The aging-program gene set was from DEMAGALHAES_AGEING_UP (26) in MSigDB. One thousand gene set permutations were performed. FDR less than 0.05 was used for enriched terms, as is recommended when performing permutations by gene set.

R version 3.5.0 was used. The RNA-Seq data are available in the NCBI's Gene Expression Omnibus (GEO) repository under accession number GSE130419.

Immunoblotting and immunoprecipitation. Cells were lysed in NP-40 lysis buffer (1% NP-40, 50 mM Tris at pH 7.5, 150 mM NaCl, 10% glycerol) containing protease inhibitor cocktail (Roche Molecular Biochemicals). The crude lysates were cleared by centrifugation at 21,130*g* at 4°C for 15 minutes. Cell lysate was treated with 2× Laemmli sample buffer (Bio-Rad, 1610737) and incubated at 95°C for 5 minutes. Protein extracts were resolved by AnyKD SDS-PAGE gel (Bio-Rad, 4569034), transferred to a PVDF membrane (MilliporeSigma), and analyzed by immunoblotting with the following antibodies: β-actin (Santa Cruz Biotechnology, I-19), Western blot (1:2000); DCAF1 (ProteinTech, 11612-1-AP), Western blot (1:2000), IP (1:200); GSTP1 (Invitrogen, Thermo Fisher Scientific, PA5-29558), Western blot (1:1000); pan-ERK (BD Biosciences, 610123), Western blot (1:2000); p-ERK (Cell Signaling Technology, 4370), Western blot (1:2000); total STAT5 (Cell Signaling Technology, 9358), Western blot (1:2000); p-STAT5 (Cell Signaling Technology, 4322), Western blot (1:2000). Full, uncut gels are included in the published online supplemental material.

For immunoprecipitation of endogenous DCAF1 and GSTP1 in mouse T cells, $CD4^+$ T cells were purified by MACS and activated by anti-CD3 and anti-CD28 for 24 hours. The cells were treated with MG132 for 4 hours before harvest. Cells were lysed in NP-40 lysis buffer (1% NP-40, 50 mM Tris at pH 7.5, 150 mM NaCl, 10% glycerol) containing protease inhibitor cocktail (Roche Molecular Biochemicals) and MG132, and rude lysates were cleared by centrifugation at 21,130*g* at 4°C for 15 minutes. The soluble fraction was divided into 2 parts and incubated with magnetic beads that conjugated with DCAF1 antibody (ProteinTech, 11612-1-AP) or rabbit IgG in a cold room overnight. The immunocomplex was washed 4 times with NP-40 lysis buffer and then 3 times with PBS. Associated proteins were eluted by 2× Laemmli sample buffer (Bio-Rad, 1610737) and incubated at 95°C for 5 minutes. The eluted proteins were resolved in SDS-PAGE gel (Bio-Rad, 4569034). For immunoprecipitation of overexpressed DCAF1 and GSTP1 in 293T cells, the cell lysate from 293T cells transfected with pCDNA-MYC-DCAF1 and MIT-FLAG-GSTP1 plasmids was prepared and subjected to immunoprecipitation with FLAG M2 beads (MilliporeSigma, M8823).

GSTP1 ubiquitylation assay. For the GSTP1 ubiquitylation assay, 293T cells were transfected with plasmid of MYC-DCAF1, FLAG-GSTP1, and HA-ubiquitin as indicated for 48 hours and treated with 100 μM proteasome inhibitor MG132 (Santa Cruz Biotechnology, sc-201270A) for an additional 4 hours before harvest. Lysates were prepared with NP-40 lysis buffer, denatured in 1% of SDS, and diluted 10-fold before immunoprecipitation. FLAG-GSTP1 was immunoprecipitated with anti-FLAG (MilliporeSigma, M2) antibody and analyzed by immunoblot with anti-HA (Roche, 3F10), anti-MYC (MilliporeSigma, 4A6), and anti-FLAG (MilliporeSigma, M2) antibodies as indicated.

GST activity assay. GST activity was analyzed by the increase of the absorbance at 340 nm at 25°C with reduced GSH and 1-chloro-2,4-dinitrobenzene (CDNB) as substrates. The GST Assay Kit (MilliporeSigma, CS0410) was used per the manufacturer's protocols. Briefly, 1 million cells were lysed in 50 μL of sample buffer by sonication. Then 30 μL of the samples were added into the assay cocktail (150 μL of PBS at pH 6.5, 10 μL of 100 mM CDNB, and 10 μL of 100 mM GSH) in 96-well plates and immediately analyzed in a plate reader. The change in absorbance (ΔA_{340}) per minute, in the linear range of the plot, was calculated using Equation 1:

$$(\Delta A_{340})/\text{min} = [A_{340}(\text{final read}) - A_{340}(\text{initial read})]/\text{reaction time (min)}$$

GST-specific activity per million cells (μmol/million/min) was calculated using Equation 2:

$$[(\Delta A_{340})/\text{min} \times V(\text{mL}) \times \text{dilution}]/[\varepsilon_{mM} \times V_{enz}(\text{mL}) \times \text{density}]$$

For our assay using 96-well plates, ε_{mM} = 5.3 mM^{-1}; V(mL) = 0.2 mL; V_{enz}(mL) = the volume of the enzyme sample tested; and density = number of cells used in cell lysate.

Histology. Tissues were resected and fixed in 4% formalin for 1 week, cleared with xylene, and embedded in paraffin. Sections of 5 μm thickness were collected and stained with H&E. The sections were examined under a microscope, and an aggregation of more than 50 mononuclear cells in the tissue was marked as lymphocytic infiltration.

Data availability. The RNA-Seq data supporting the findings of this study were deposited in the NCBI's GEO under accession number GSE130419. The IP-MS proteomics data supporting the findings of this study were deposited in the ProteomeXchange Consortium via the PRoteomics IDEntification partner repository with the data set identifier PXD003180 (34). The published data for proteome changes during mouse brain aging were from PXD005230 (32).

Statistics. Data analysis was performed and grafted by Prism (GraphPad Software Inc.). Statistical significance was determined by Mann-Whitney *U* test, 2-tailed Student's *t* test, 1-way ANOVA followed by Tukey's multiple-comparisons test, and 2-way ANOVA followed by Holm-Šidák multiple-comparisons test as indicated. A *P* value of less than 0.05 (confidence interval of 95%) was considered significant. In the figures, asterisks are used to indicate *P* values as follows: $P > 0.05$, $^{*}P < 0.05$, $^{**}P < 0.01$, $^{***}P < 0.001$, $^{****}P < 0.0001$. The sample sizes (*n*) are stated in the figure legends to indicate biologically independent replicates used for statistical analysis.

Study approval. All mouse experiments in this study were approved by the Institutional Animal Care and Use Committee of the University of North Carolina at Chapel Hill.

Author contributions

ZG designed and performed cellular, molecular, biochemical, bioinformatics, and animal experiments, and wrote the manuscript. GW and JZ contributed to RNA-Seq experiments. BW contributed to Treg proliferation experiments. WCC and JPYT contributed to colitis experiments. LC and LS contributed to human T cell experiments. JL and DW contributed to bioinformatics analysis. CZ contributed critical reagents for aging analysis. YYW conceived the project, designed experiments, and wrote the manuscript.

Acknowledgments

We thank Nancy Fisher and Janet Dow (University of North Carolina Flow Cytometry facility, supported in part by P30-CA016086 Cancer Center Core Support Grant) for cell sorting; Cheng Chris Fan (University of North Carolina) for bioinformatics analysis; Yue Xiong for providing *Dcaf1*$^{fl/fl}$ mice; and Yuan Zhuang for critical reading of the manuscript. This study was supported by the NIH (R01-MH101819-01; P30-ES010126) to DW; by the NIH (R01-AI029564) and the National Multiple Sclerosis Society (CA10068) to JPYT; and by the NIH (AI123193) and the National Multiple Sclerosis Society (RG-1802-30483) to YYW.

Address correspondence to: Yisong Y. Wan, Lineberger Comprehensive Cancer Center, Department of Microbiology and Immunology, University of North Carolina at Chapel Hill, 125 Mason Farm Road, Chapel Hill, North Carolina 27599-7599, USA. Phone: 919.966.9728; Email: wany@email.unc.edu.

1. Fulop T, et al. Immunosenescence and inflamm-aging as two sides of the same coin: friends or foes? *Front Immunol*. 2017;8:1960.
2. Partridge L, Deelen J, Slagboom PE. Facing up to the global challenges of ageing. *Nature*. 2018;561(7721):45–56.
3. Franceschi C, Campisi J. Chronic inflammation (inflammaging) and its potential contribution to age-associated diseases. *J Gerontol A Biol Sci Med Sci*. 2014;69(suppl 1):S4–S9.
4. Kennedy BK, et al. Geroscience: linking aging to chronic disease. *Cell*. 2014;159(4):709–713.
5. Ovadya Y, et al. Impaired immune surveillance accelerates accumulation of senescent cells and aging. *Nat Commun*. 2018;9(1):5435.
6. Furman D, et al. Chronic inflammation in the etiology of disease across the life span. *Nat Med*. 2019;25(12):1822–1832.
7. Milikovsky DZ, et al. Paroxysmal slow cortical activity in Alzheimer's disease and epilepsy is associated with blood-brain barrier dysfunction. *Sci Transl Med*. 2019;11(521):eaaw8954.
8. Senatorov VV, et al. Blood-brain barrier dysfunction in aging induces hyperactivation of TGFβ signaling and chronic yet reversible neural dysfunction. *Sci Transl Med*. 2019;11(521):eaaw8283.
9. Mahmoudi S, Xu L, Brunet A. Turning back time with emerging rejuvenation strategies. *Nat Cell Biol*. 2019;21(1):32–43.
10. Nikolich-Zugich J. Aging of the T cell compartment in mice and humans: from no naive expectations to foggy memories. *J Immunol*. 2014;193(6):2622–2629.
11. Thome JJ, et al. Spatial map of human T cell compartmentalization and maintenance over decades of life. *Cell*. 2014;159(4):814–828.
12. Wing K, Sakaguchi S. Regulatory T cells exert checks and balances on self tolerance and autoimmunity. *Nat Immunol*. 2010;11(1):7–13.
13. Sakaguchi S, Yamaguchi T, Nomura T, Ono M. Regulatory T cells and immune tolerance. *Cell*. 2008;133(5):775–787.
14. Nikolich-Žugich J. The twilight of immunity: emerging concepts in aging of the immune system. *Nat Immunol*. 2018;19(1):10–19.
15. Boraschi D, et al. The gracefully aging immune system. *Sci Transl Med*. 2013;5(185):185ps8.
16. Fessler J, Ficjan A, Duftner C, Dejaco C. The impact of aging on regulatory T-cells. *Front Immunol*. 2013;4:231.
17. Gregg R, et al. The number of human peripheral blood CD4+ CD25high regulatory T cells increases with age. *Clin Exp Immunol*. 2005;140(3):540–546.
18. Nishioka T, Shimizu J, Iida R, Yamazaki S, Sakaguchi S. CD4+CD25+Foxp3+ T cells and CD4+CD25-Foxp3+ T cells in aged mice. *J Immunol*. 2006;176(11):6586–6593.
19. Vukmanovic-Stejic M, et al. Human CD4+ CD25hi Foxp3+ regulatory T cells are derived by rapid turnover of memory populations in vivo. *J Clin Invest*. 2006;116(9):2423–2433.
20. Zhao L, Sun L, Wang H, Ma H, Liu G, Zhao Y. Changes of CD4+CD25+Foxp3+ regulatory T cells in aged Balb/c mice. *J Leukoc Biol*. 2007;81(6):1386–1394.
21. Kuswanto W, et al. Poor repair of skeletal muscle in aging mice reflects a defect in local, interleukin-33-dependent accumulation of regulatory T cells. *Immunity*. 2016;44(2):355–367.
22. Jagger A, Shimojima Y, Goronzy JJ, Weyand CM. Regulatory T cells and the immune aging process: a mini-review. *Gerontology*. 2014;60(2):130–137.
23. Chougnet CA, et al. A major role for Bim in regulatory T cell homeostasis. *J Immunol*. 2011;186(1):156–163.
24. Raynor J, et al. IL-6 and ICOS antagonize Bim and promote regulatory T cell accrual with age. *J Immunol*. 2015;195(3):944–952.
25. Sharpless NE, Sherr CJ. Forging a signature of in vivo senescence. *Nat Rev Cancer*. 2015;15(7):397–408.
26. de Magalhães JP, Curado J, Church GM. Meta-analysis of age-related gene expression profiles identifies common signatures of aging. *Bioinformatics*. 2009;25(7):875–881.
27. Garg SK, et al. Aging is associated with increased regulatory T-cell function. *Aging Cell*. 2014;13(3):441–448.
28. Lages CS, et al. Functional regulatory T cells accumulate in aged hosts and promote chronic infectious disease reactivation. *J Immunol*. 2008;181(3):1835–1848.
29. Sun L, et al. Aged regulatory T cells protect from autoimmune inflammation despite reduced STAT3 activation and decreased constraint of IL-17 producing T cells. *Aging Cell*. 2012;11(3):509–519.
30. Mottet C, Uhlig HH, Powrie F. Cutting edge: cure of colitis by CD4+CD25+ regulatory T cells. *J Immunol*. 2003;170(8):3939–3943.
31. Chang J, et al. Clearance of senescent cells by ABT263 rejuvenates aged hematopoietic stem cells in mice. *Nat Med*. 2016;22(1):78–83.
32. Duda P, Wojcicka O, Wisniewski JR, Rakus D. Global quantitative TPA-based proteomics of mouse brain structures reveals significant alterations in expression of proteins involved in neuronal plasticity during aging. *Aging (Albany NY)*. 2018;10(7):1682–1697.
33. Zhang S, Feng Y, Narayan O, Zhao LJ. Cytoplasmic retention of HIV-1 regulatory protein Vpr by protein-protein interaction with a novel human cytoplasmic protein VprBP. *Gene*. 2001;263(1-2):131–140.
34. Guo Z, et al. DCAF1 controls T-cell function via p53-dependent and -independent mechanisms. *Nat Commun*. 2016;7:10307.
35. Gross AM, et al. Methylome-wide analysis of chronic HIV infection reveals five-year increase in biological age and epigenetic targeting of HLA. *Mol Cell*. 2016;62(2):157–168.

36. Nelson JA, et al. Expression of p16(INK4a) as a biomarker of T-cell aging in HIV-infected patients prior to and during antiretroviral therapy. *Aging Cell*. 2012;11(5):916–918.
37. Rufini A, Tucci P, Celardo I, Melino G. Senescence and aging: the critical roles of p53. *Oncogene*. 2013;32(43):5129–5143.
38. Horvath S, Levine AJ. HIV-1 infection accelerates age according to the epigenetic clock. *J Infect Dis*. 2015;212(10):1563–1573.
39. Chiappini E, et al. Accelerated aging in perinatally HIV-infected children: clinical manifestations and pathogenetic mechanisms. *Aging (Albany NY)*. 2018;10(11):3610–3625.
40. Rincon M. MAP-kinase signaling pathways in T cells. *Curr Opin Immunol*. 2001;13(3):339–345.
41. Lanna A, et al. A sestrin-dependent Erk-Jnk-p38 MAPK activation complex inhibits immunity during aging. *Nat Immunol*. 2017;18(3):354–363.
42. Shapiro-Shelef M, Lin KI, Savitsky D, Liao J, Calame K. Blimp-1 is required for maintenance of long-lived plasma cells in the bone marrow. *J Exp Med*. 2005;202(11):1471–1476.
43. Cagnol S, Chambard JC. ERK and cell death: mechanisms of ERK-induced cell death--apoptosis, autophagy and senescence. *FEBS J*. 2010;277(1):2–21.
44. Franchina DG, Dostert C, Brenner D. Reactive oxygen species: involvement in T cell signaling and metabolism. *Trends Immunol*. 2018;39(6):489–502.
45. Colavitti R, Finkel T. Reactive oxygen species as mediators of cellular senescence. *IUBMB Life*. 2005;57(4-5):277–281.
46. Finkel T, Holbrook NJ. Oxidants, oxidative stress and the biology of ageing. *Nature*. 2000;408(6809):239–247.
47. Nakagawa T, et al. CRL4(VprBP) E3 ligase promotes monoubiquitylation and chromatin binding of TET dioxygenases. *Mol Cell*. 2015;57(2):247–260.
48. Coles BF, Kadlubar FF. Detoxification of electrophilic compounds by glutathione S-transferase catalysis: determinants of individual response to chemical carcinogens and chemotherapeutic drugs? *Biofactors*. 2003;17(1-4):115–130.
49. Dang DT, Chen F, Kohli M, Rago C, Cummins JM, Dang LH. Glutathione S-transferase pi1 promotes tumorigenicity in HCT116 human colon cancer cells. *Cancer Res*. 2005;65(20):9485–9494.
50. Ayyadevara S, et al. Lifespan and stress resistance of Caenorhabditis elegans are increased by expression of glutathione transferases capable of metabolizing the lipid peroxidation product 4-hydroxynonenal. *Aging Cell*. 2005;4(5):257–271.
51. Coussens LM, Werb Z. Inflammation and cancer. *Nature*. 2002;420(6917):860–867.
52. Dulken BW, et al. Single-cell analysis reveals T cell infiltration in old neurogenic niches. *Nature*. 2019;571(7764):205–210.
53. Deeks SG, Phillips AN. HIV infection, antiretroviral treatment, ageing, and non-AIDS related morbidity. *BMJ*. 2009;338:a3172.
54. Maj T, et al. Oxidative stress controls regulatory T cell apoptosis and suppressor activity and PD-L1-blockade resistance in tumor. *Nat Immunol*. 2017;18(12):1332–1341.
55. Mak TW, et al. Glutathione primes T cell metabolism for inflammation. *Immunity*. 2017;46(4):675–689.
56. Ray PD, Huang BW, Tsuji Y. Reactive oxygen species (ROS) homeostasis and redox regulation in cellular signaling. *Cell Signal*. 2012;24(5):981–990.
57. Mannick JB, et al. mTOR inhibition improves immune function in the elderly. *Sci Transl Med*. 2014;6(268):268ra179.
58. McCall CM, et al. Human immunodeficiency virus type 1 Vpr-binding protein VprBP, a WD40 protein associated with the DDB1-CUL4 E3 ubiquitin ligase, is essential for DNA replication and embryonic development. *Mol Cell Biol*. 2008;28(18):5621–5633.
59. Lee PP, et al. A critical role for Dnmt1 and DNA methylation in T cell development, function, and survival. *Immunity*. 2001;15(5):763–774.
60. Debacq-Chainiaux F, Erusalimsky JD, Campisi J, Toussaint O. Protocols to detect senescence-associated beta-galactosidase (SA-betagal) activity, a biomarker of senescent cells in culture and in vivo. *Nat Protoc*. 2009;4(12):1798–1806.
61. Jackson SH, Devadas S, Kwon J, Pinto LA, Williams MS. T cells express a phagocyte-type NADPH oxidase that is activated after T cell receptor stimulation. *Nat Immunol*. 2004;5(8):818–827.
62. Patro R, Duggal G, Love MI, Irizarry RA, Kingsford C. Salmon provides fast and bias-aware quantification of transcript expression. *Nat Methods*. 2017;14(4):417–419.
63. Soneson C, Love MI, Robinson MD. Differential analyses for RNA-seq: transcript-level estimates improve gene-level inferences. *F1000Res*. 2015;4:1521.
64. Love MI, Huber W, Anders S. Moderated estimation of fold change and dispersion for RNA-seq data with DESeq2. *Genome Biol*. 2014;15(12):550.
65. Subramanian A, et al. Gene set enrichment analysis: a knowledge-based approach for interpreting genome-wide expression profiles. *Proc Natl Acad Sci U S A*. 2005;102(43):15545–15550.
66. Liberzon A, Subramanian A, Pinchback R, Thorvaldsdóttir H, Tamayo P, Mesirov JP. Molecular signatures database (MSigDB) 3.0. *Bioinformatics*. 2011;27(12):1739–1740.